Geophysical Journal International

Geophys. J. Int. (2025) **243,** 1–24
Advance Access publication 2025 August 07
Research Paper

https://doi.org/10.1093/gji/ggaf293

Age dependent variation of the magnetic fabric of dike swarms and implications for the volcanic structure of ocean islands: the example of the Maio Island, Cabo Verde archipelago

Mário Moreira,[1,2] João Mata,[2,3] José Madeira,[2,3] Patrícia Represas[4] and Sofia Martins[3]

[1]*Departamento de Física, Instituto Superior de Engenharia de Lisboa (ISEL), Instituto Politécnico de Lisboa,* rua Conselheiro Emídio Navarro 1, 1959-007 *Lisboa, Portugal. E-mail: mario.moreira@isel.pt*
[2]*Instituto Dom Luiz (IDL), Faculdade de Ciências, Universidade de Lisboa,* 1749-016 *Lisboa, Portugal*
[3]*Departamento de Geologia, Faculdade de Ciências, Universidade de Lisboa,* 1749-016 *Lisboa, Portugal*
[4]*Laboratório Nacional de Energia e Geologia (LNEG), Estrada da Portela, Zambujal, Apartado* 7586, 2611-901 *Amadora, Portugal*

Accepted 2025 July 19. Received 2025 July 17; in original form 2025 January 13

SUMMARY

Magnetic fabric analysis of dikes is a powerful technique when assessing magma transfer processes. This study presents an integrated analysis combining magnetic susceptibility and anisotropy of magnetic susceptibility, magnetic mineralogy, geochemistry and new $^{40}Ar/^{39}$ Ar dating of dikes intruding formations ranging from the Lower Cretaceous to the Miocene on the island of Maio, in the Cabo Verde archipelago. We show that the dikes, dated at ≈9.2 Ma, intruding the younger Miocene Casas Velhas formation, display a Ti-rich titanomagnetite composition, higher whole-rock TiO_2 content and very high magnetic anisotropy. They are clearly distinguished from the dikes, ranging in age from ≈9.3 to 11.3 Ma, intruding older formations, which show a predominantly Ti-poor titanomagnetite composition with multiple magnetic phases, lower whole-rock TiO_2 concentration, higher range of magnetic susceptibilities and very low anisotropy. Magnetic fabric is predominantly normal with no significant imbrication relative to the dike margins. Numerical analysis of fabric shows a dominant coaxiality between the magnetic lineation and the preferred orientation of opaques and phenocrystals suggesting that magnetic lineation is, therefore, the proxy of the magmatic flow axis orientation. Based on the orientation of the magnetic fabric, we infer that magmatic flow within the studied dikes is predominantly vertical. The differences observed between the younger dikes and all other dikes may be related to magma sourced from distinct magma chambers. One, probably shallow, underneath the Casas Velhas fm in the southwest of the island, which would explain the very high values of magnetic anisotropy and the inferred vertical flow, and another located in a central position in the island, responsible for the dikes intruding the older formations. The location of such magma reservoirs and the dikes ages suggest a hypothetical migration with age of the magmatic sources that fed the dikes from the central part of the island to the southwest region. The magnetic and mineralogical heterogeneities of the dikes intruding older Lower Cretaceous formations may also be a result of a wider age range of the intrusions.

Key words: Magnetic fabrics and anisotropy; Magnetic mineralogy and petrology; Atlantic Ocean; Physics and chemistry of magma bodies.

1 INTRODUCTION

The study of magmatic dikes by rock magnetic techniques, when focussed on magma flow characterization, greatly improve the understanding of shallow level magmatic processes. Dikes provide valuable information on temporal and spatial magma transfer process with sill-like bodies being considered the cause for endogenous growth of volcanic ocean islands (e.g. Klugel *et al.* 2015; Ramalho *et al.* 2017). Their geometry, orientation and distribution are linked to the local stress regime as they propagate and intrude through the country rocks, opening fractures along the direction of minimum tectonic stress. Furthermore, dikes contain information

of the physical and geochemical process experienced by the magma during its flow path, from the magma reservoir through the crust and up to the surface.

The interpretation of the magnetic fabric, obtained from the anisotropy of magnetic susceptibility (AMS), provides an objective and quantitative tool to interpret the fossil magmatic-flow pattern geometry, providing a characterization of their emplacement and intrusion mode.

This work was developed in Maio, one of the oldest and most eroded islands of the Cabo Verde Archipelago, being characterized by a complex geologic history with outcropping formations ranging from the Lower Cretaceous to the Holocene (e.g. Serralheiro 1970; Stillman *et al.* 1982; Azéma *et al.* 1990; Holm *et al.* 2008; Madeira *et al.* 2020; Samrock *et al.* 2022).

Based on the structural attitude (strike and dip direction) of 290 planar intrusions, we sampled 26 mafic dikes and one carbonatite dike, intruding Mid-Ocean Ridge Basalts (MORB) pillows from the Lower Cretaceous 'Batalha formation', the thin-bedded limestones and shales of 'Carqueijo formation' and the submarine to subaerial lavas sequence of the Miocene 'Casas Velhas formation'.

The magnetic mineral characterization included the determination of Curie temperatures of magnetic phases and determination of coercivities of remanence (isothermal remanence magnetization). Twenty whole-rock samples were analysed for major and trace elements, which in conjunction with electron microprobe analyses of the main mineral phases, allowed a characterization of the dikes. To constrain the age of the different dike families, we present six new $^{40}Ar/^{39}Ar$ dates. The study of the AMS allowed the characterization and differentiation of the dikes intruding the different formations. To correlate the magnetic fabric obtained from the AMS, with the magmatic flow fabric, we performed image analysis of different mineral phases on oriented thin section of rock through the intercept method (Launeau & Robin 1996).

2 CABO VERDE ARCHIPELAGO AND MAIO ISLAND: GEOLOGICAL AND GEOPHYSICAL SETTING

The Cabo Verde archipelago (Fig. 1) in the Atlantic Ocean lies 700 km offshore the coast of Senegal, West Africa. The archipelago stands on a mid-plate topographic swell—the Cabo Verde Rise, considered to be the largest within-plate bathymetric anomaly in oceanic basins with an amplitude ≈2.2 km and a diameter of 1400–1600 km. The Cabo Verde Rise is associated with pronounced geoid, gravimetric and heat flow anomalies (e.g. Dash *et al.* 1976; Courtney & White 1986) compatible with those believed to be originated by the impingement of mantle plumes on lithospheric plates (e.g. Sleep 1990), which has been confirmed by seismic data (e.g. Liu & Zhao 2014; Carvalho *et al.* 2019; 2021). Moreover, the thinning of the mantle transition zone (Vinnik *et al.* 2012) point to an origin of the mantle plume in the lower mantle, which, according to seismic tomography (Montelli *et al.* 2006) and noble gas analysis (e.g. Mata *et al.* 2010; Mourão *et al.* 2012), must be rooted in its deepest levels.

In the Cabo Verde archipelago, the oldest age determined on alkaline intraplate magmatism was obtained in submarine basalts from the basal complex of the Island of Sal (Torres *et al.* 2010) dated at 25.6 Ma. The youngest eruption in Cabo Verde occurred on Fogo Island in 2014−2015 (Gonzalez *et al.* 2015; Mata *et al.* 2017).

Magnetic anomalies and bathymetric data indicate that the Cabo Verde islands stand on Early Cretaceous (Valanginian) oceanic crust, between the magnetic anomalies M0 to M16. Maio Island is located roughly between magnetic anomalies M11 (≈136 Ma) and M16 (≈141 Ma) (Hayes & Rabinowitz 1975; Stilman *et al.* 1982; Fourcade *et al.* 1990).

The first full stratigraphic description of Maio Island was produced by Serralheiro (1970) and later revised and refined by Stillman *et al.* (1982), Casson *et al.* (2020) and Samrock *et al.* (2022). It may be summarized (Fig. 2) considering three major geological units: (1) an old, Lower Cretaceous, raised sea-floor sequence (Mesozoic Basement Complex—MBC), comprising mid-ocean ridge basaltic pillow lavas and breccias (MORB; Paepe *et al.* 1974), the Batalha formation (fm.), covered by Cretaceous deep marine carbonated and marly fossiliferous sediments, the Morro, Carqueijo fm. and Coruja fm. (Serralheiro 1970; Paepe *et al.* 1974); (2) a Paleogene intrusive alkaline complex (Central Igneous Complex—CIC), composed of essexites/pyroxenites and minor nepheline monzosyenites (e.g. Villaseca *et al.* 2025) forming a dome-like structure in the older rocks and representing exhumed magma chambers (Represas *et al.* 2012), and; (3) a sequence of initially submarine, then subaerial, extrusive volcanic formations and sediments (Casas Velhas, Pedro Vaz, Malhada Pedra, and Monte Penoso formations.), with volcanics of Malhada Pedra fm. and Monte Penoso fm. being considered by Samrock *et al.* (2022), the result of decompression-induced mantle melting as a consequence of significant island flank collapses occurred at 8.7 to 6.7 Ma. A sequence of Plio-quaternary deposits, including a staircase of raised beach deposits, aeolian calcarenites, tsunami conglomerates and sandstones, recent alluvial fan deposits, aeolian sands and sabkha sediments partially cover the main volcano-sedimentary units (Ramalho *et al.* 2010; Madeira *et al.* 2020).

3 ANALYTICAL METHODS

3.1 Magnetic susceptibility and anisotropy (AMS)

The physics of magnetism and physical interpretation of magnetic susceptibility has been extensively described in several textbooks and articles (e.g. Tarling & Hrouda 1993; Dunlop & Özdemir 1997) and the meaning of magnetic parameters has been previously well summarized. The magnetic susceptibility k is defined as the ratio of magnetization M (magnetic moment per unit volume, A/m) to the applied magnetic field intensity H (A/m). For relatively low applied fields this relationship is practically linear. It is therefore a dimensionless quantity.

The anisotropy of magnetic susceptibility represents the directional dependence of the magnetic susceptibility in a material and may be defined equating the magnetic susceptibility values in the three mutually perpendicular directions. The AMS is described by three different eigenvectors, $k_1 > k_2 > k_3$, that characterize the three orthogonal axes of the susceptibility ellipsoid, designated as maximum, intermediate, and minimum susceptibilities, respectively. These magnetic axes commonly align coaxially with the principal axes of finite strain according to the geological conditions and stress field, defining a magnetic fabric.

The principal susceptibilities k_1, k_2 and k_3 and their relationships are used to define several parameters relating shape and magnitude. Most common parameters are the bulk susceptibility $k = (k_1 + k_2 + k_3)/3$, the degree of magnetic lineation $L = (k_1 - k_2)/k_1$, and the degree of magnetic foliation $F = (k_2 - k_3)/k_1$, (Khan 1962).

The shape of the AMS ellipsoid may vary between a flattened or oblate shape to an elongated or prolate shape. The shape parameter,

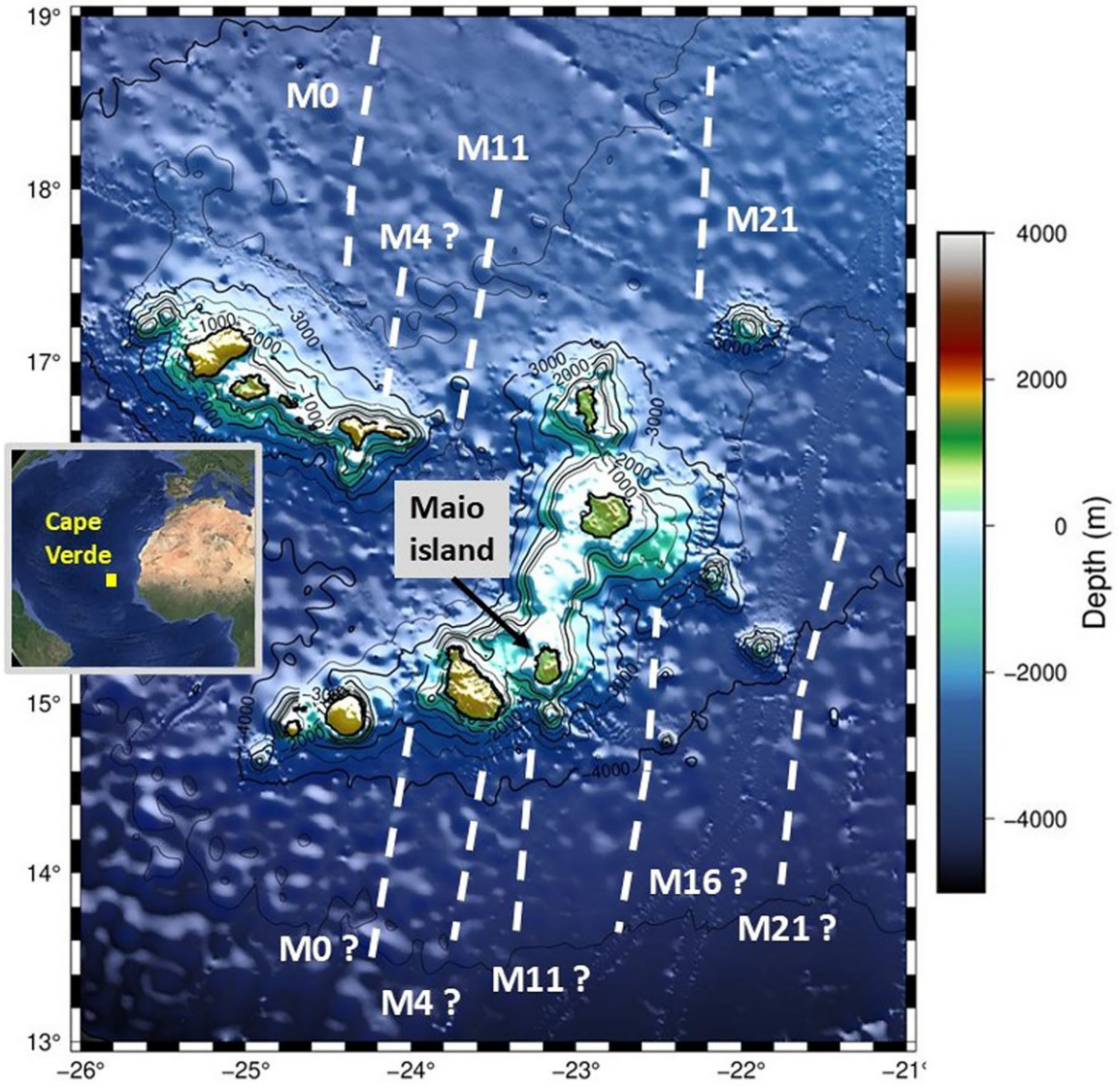

Figure 1. Bathymetry of the Cabo Verde Rise (produced with GMT—Unix software package and GEBCO global relief grid, 1 min × 1 min; Compilation Group (2024) GEBCO 2024 Grid—https://doi.org/10.5285/1c44ce99-0a0d-5f4f-e063-7086abc0ea0f) and approximate locations of crustal magnetic anomalies M0–M21 marked by dashed lines based on Pim *et al.* (2008); the inset shows the geographical location of the Cabo Verde Archipelago (Google Earth image, April 2024).

T (Jelinek 1981) is defined as $T = (2\eta_2 - \eta_1 - \eta_3)/(\eta_1 - \eta_3)$, where $\eta_1 = \ln k_1$, $\eta_2 = \ln k_2$, and $\eta_3 = \ln k_3$. In this sense T varies between -1 and 1. A positive T value means that the specimen has oblate shape while a negative T value indicates prolate shape. Anisotropy of MS may be expressed as a scalar $P = k_1/k_3$ and, more accurately, as the Corrected Degree of Anisotropy P_j (Jelinek 1981), defined as: $P_j = \exp(2((\ln(k_1/k_m))^2 + (\ln(k_2/k_m))^2 + (\ln(k_3/k))^2))^{1/2}$.

The anisotropy may also be mathematically expressed as a percentage, in the percentage form P per cent = 100 per cent × $(k_1 - k_3)$/k.

The low field magnetic susceptibility, currently referred to as MS, was measured with a KLY-2 Kappabridge (AC susceptibility bridge) at 300 A/m, 920 Hz. The morphology of the AMS ellipsoid was evaluated by the distribution of the MS axes through the magnetic anisotropy data analysis program Anisoft (from Agico–Chadima & Jelinek 2008) with the mean tensors and principal directions, under the 95 per cent confidence ellipses calculated by the Jelinek statistics (Jelinek 1978).

3.2 Thermomagnetic analysis

Thermomagnetic curves were performed to identify ferromagnetic (s.l.) minerals based on their Curie temperature. High temperature heating-cooling cycles up to ≈650 °C were performed on a CS4 furnace, connected to a MFK1 Kappabridge (Agico) operating at a field of 200 A/m, and a frequency of 976 Hz. Heating and cooling rates were 9 °C min^{-1}. The experiments were executed in Argon controlled atmosphere to minimize the oxidation of the samples during heating.

3.3 Isothermal remanent magnetization and coercivity of remanence

The characterization of the coercivities of the magnetic minerals was obtained through isothermal remanence magnetization (IRM) curves. The saturation of remanent magnetization (SIRM) and the associated back field demagnetization were measured to provide

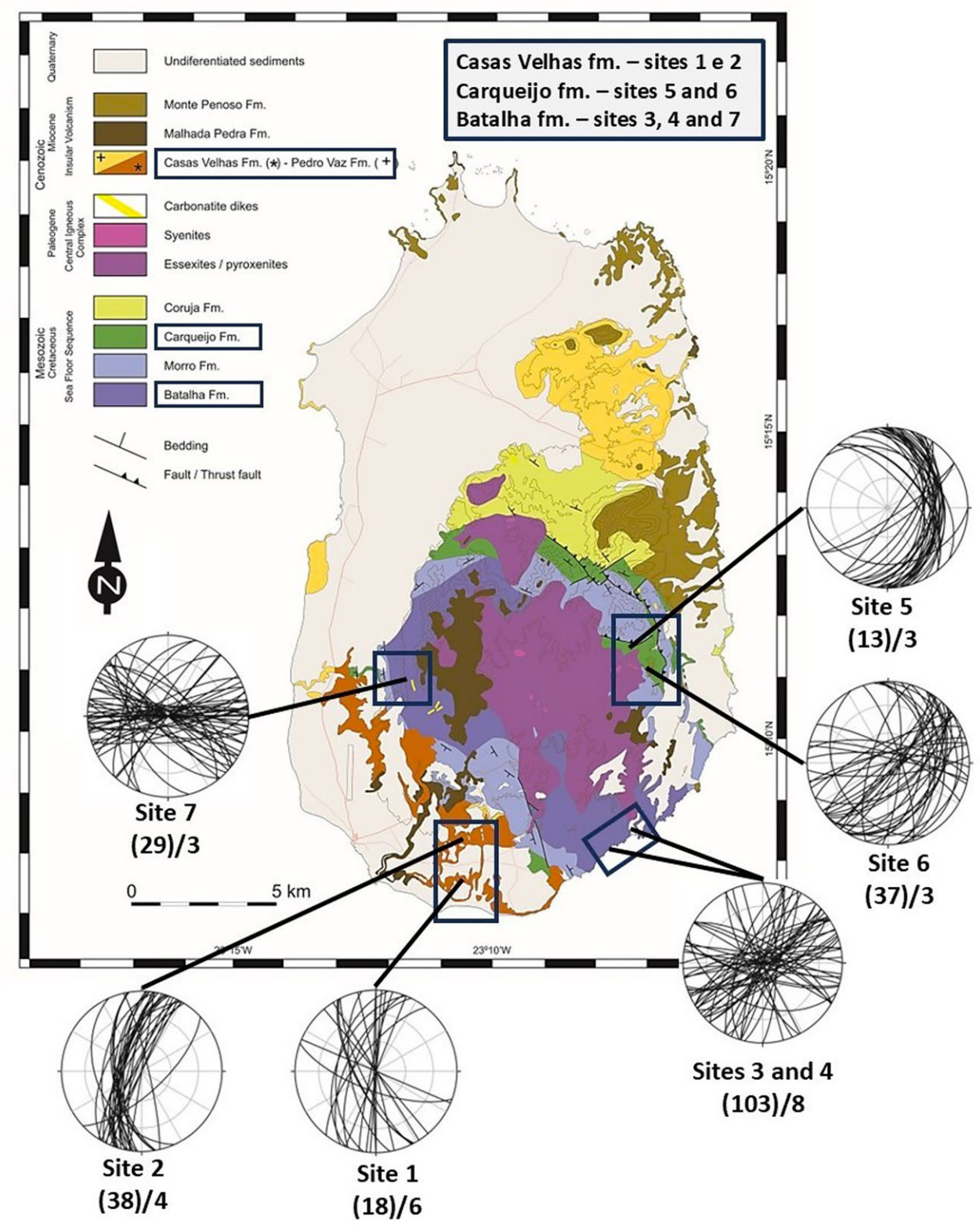

Figure 2. Simplified geological map compiled from Serralheiro (1970) and Stillman *et al.* (1982) with the main geological formations and the location of magnetic sampling sites. For each sampling site the stereographic projection of dike attitudes is represented including the number of all identified dikes, (in parenthesis), and the number of studied dikes.

information on both the dominant domain state of the magnetic fraction and on the characterization of magnetic coercivities of the material. According to Robertson & France (1994) and Kruiver *et al.* (2001) the IRM acquisition of different phases theoretically follow a log-normal distribution and are cumulative in intensity. The obtained curves can be described by three main parameters: SIRM that measures the amplitude of the magnetization at saturation, $B_{1/2}$ that measures the field at which half of the SIRM is reached, and

Table 1. Characterization of the sampling sites. The asterisk indicates the carbonatite dike.

Site	Location	Coordinates Lat. N/Long. W	Geological formation	No. of measured intrusions	Sampled intrusions
1	Barreiro, Ribeira de Cumiassa, south.	15 º 07′ 53″23 º 10′ 22″	Casas Velhas Miocene	18	1, 2, 3, 4, 5, 6
2	Barreiro, Ribeira de Cumiassa, north.	15 º 08′ 33″23 º 10′ 09″	Casas Velhas Miocene	38	13, 14, 15, 16
3	Dom João bay, west cliffs. (south of CIC)	15 º 08′ 24″23 º 07′ 21″	BatalhaLower Cretaceous	50	7, 8, 9, 10, 11
4	0.5 km west of Dom João bay. (south of CIC)	15 º 08′ 13″23 º 07′ 38″	BatalhaLower Cretaceous	53	23, 24, 25
5	1 km SW of Pilão Cão village.	15 º 12′ 07″23 º 06′ 42″	CarqueijoUpper Cretaceous	15	17, 18, 19
6	Ribeira da Baía, 2 km SSW of Pilão Cão.	15 º 11′ 21″23 º 06′ 52″	CarqueijoUpper Cretaceous	37	20, 21, 22
7	Chão do Monte (West of CIC)	15 º 10′ 28″23 º 11′ 48″	BatalhaLower Cretaceous	29	26∗, 27, 28

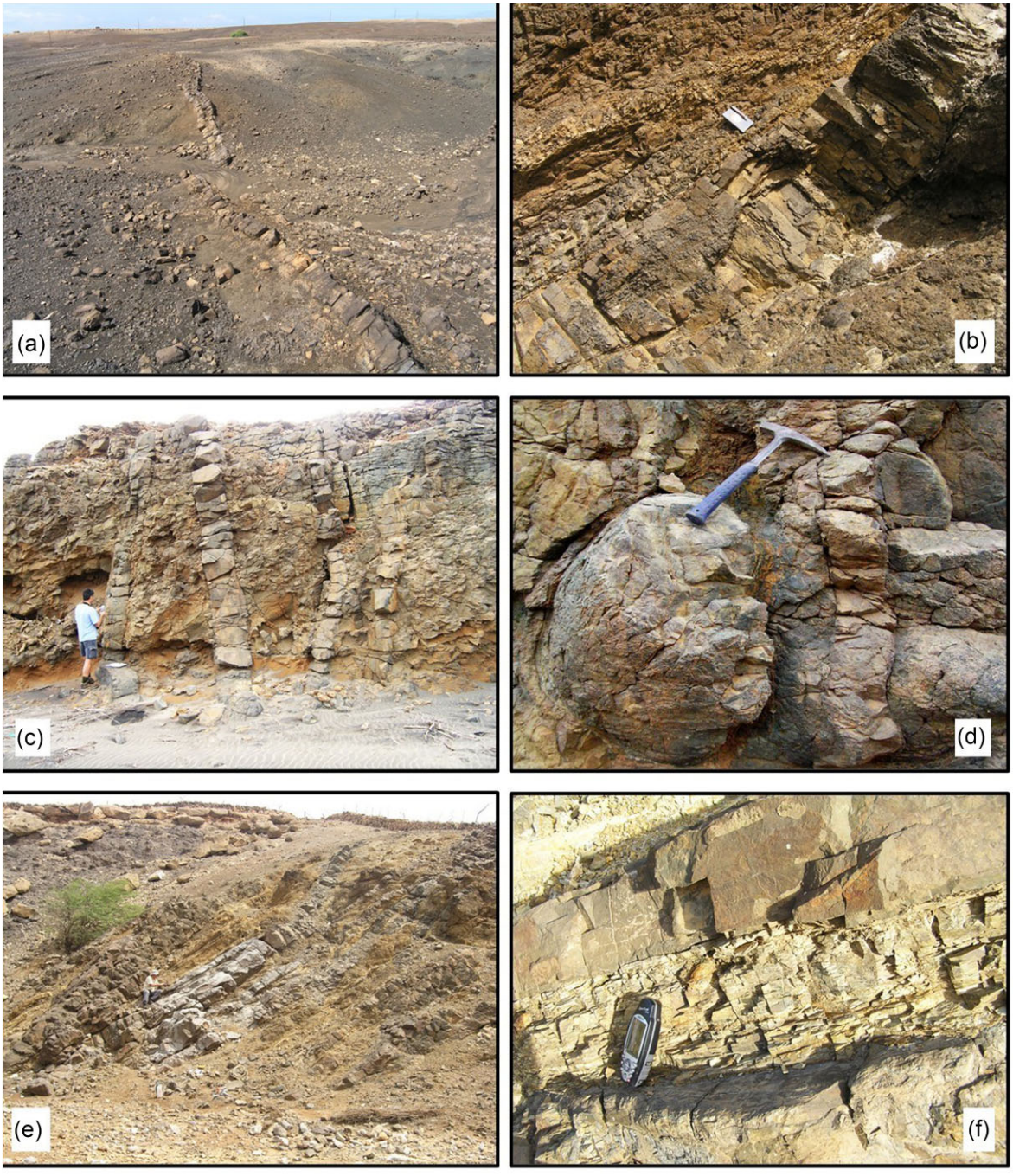

Figure 3. Field photographs of the samples sites: (a, b) dikes from Casas Velhas fm. at Ribeira de Cumiassa, (site 2); dikes are usually narrow, highly weathered and fractured; (c, d) dikes from Batalha fm.at Dom João Bay (site 3) and cutting a MORB pillow (site 4); (e, f) dikes from Carqueijo fm.at Ribeira da Baía (site 6); here, the intrusions are mostly sills typically parallel to the limestone strata. Photographs taken by the authors.

Table 2. Summary of $^{40}Ar/^{39}Ar$ ages determined on dikes groundmass.

Sample	Intruded formation	Plateau characteristics					
		Plateau age Ma ± 2 σ	No. of steps used	^{39}Ar% of total	K/Ca ± 2 σ	MSWD F	P
Ma11	Batalha Site 3	11.28 ± 0.21	6	63.36	0.387 ± 0.243	0.07	1.00
Ma15	Casas Velhas Site 2	9.24 ± 0.49	5	57.99	0.056 ± 0.044	0.04	1.00
Ma19	Carqueijo Site 5	10.12 ± 0.14	9	92.53	0.349 ± 0.156	0.06	1.00
Ma20	Carqueijo Site 6	9.34 ± 0.07	6	58.55	0.960 ± 0.789	0, 31	0.91
Ma29	Morro	9.60 ± 0.09	8	83.15	0.274 ± 0.188	0, 28	0.96
Ma30	Morro	10.18 ± 0.12	13	100	0.152 ± 0.081	0, 06	1.00

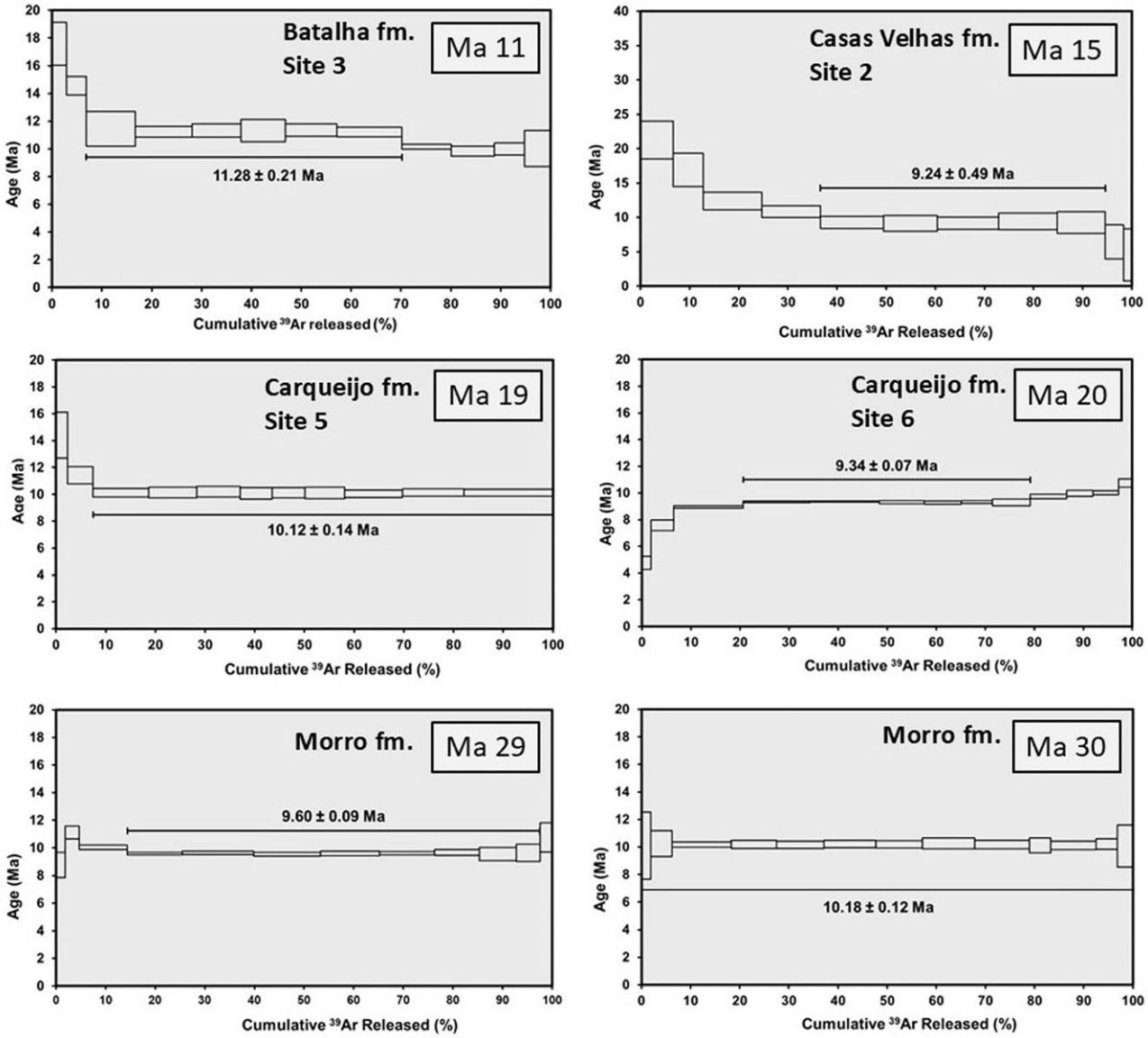

Figure 4. Step-heating $^{40}Ar/^{39}Ar$ apparent age spectra for the dated samples. Reported errors for plateau ages are 2σ. Steps used for the plateau age calculation are indicated by the horizontal black line. See also Table 2 for further information.

the dispersion parameter DP, which measures the distribution of the coercivities of the mineral phases and characterizes the homogeneity of the population in terms of grain size and composition.

Selected samples were previously demagnetized by an alternating magnetic field at 100 mT and further submitted to a progressive uniaxial and constant magnetic field up to 1 T at constant temperature, using a IM-10–30 pulse magnetizer (ASC Scientific). The resulting remanent magnetizations were measured with a JR-6 spinner magnetometer (Agico).

For the analysis of results, we used the Kruiver *et al.* (2001) software which allows fitting of $B_{1/2}$, SIRM and DP values on a linear (LAP), or gradient (GAP) plot. If more than one mineral phase is present, the theoretical curves may be fitted by more than one component.

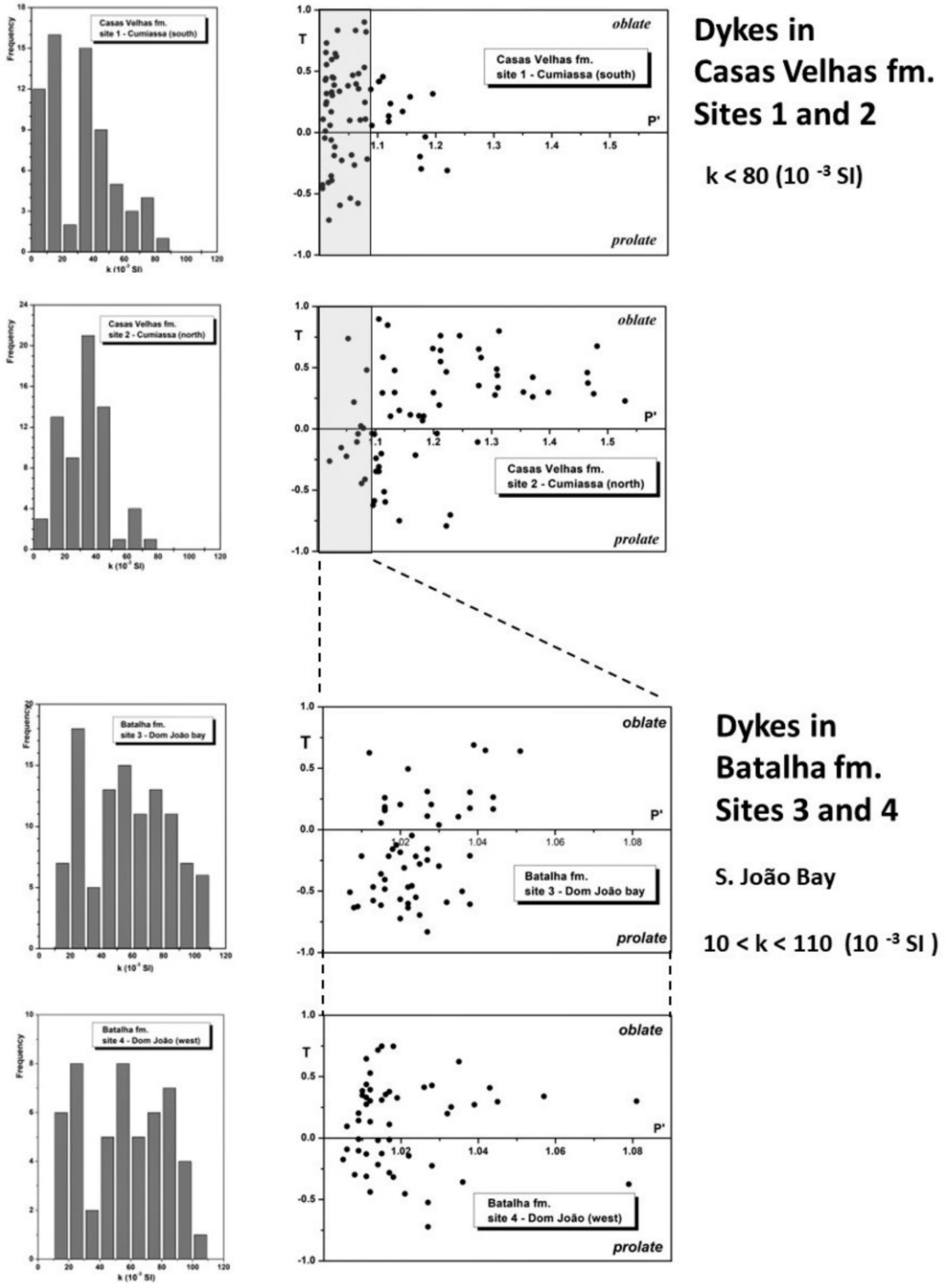

Figure 5a. Magnetic susceptibility distribution on dikes (left) and diagram of anisotropy degree P_J versus shape parameter T (right), sites 1, 2, 3, 4.

All magnetic measurements were performed at the Paleomagnetic Laboratory of the Instituto Dom Luiz at the Faculdade de Ciências da Universidade de Lisboa, Portugal.

3.4 Geochemical analyses: whole-rock major element analyses

At the Departamento de Geologia da Faculdade de Ciências da Universidade de Lisboa, samples were crushed by hydraulic press, selected after removal of all pieces with any visible signs of alteration, and then reduced in size by a jaw crusher and powdered in an agate swing mill.

Major whole rock analyses were performed at Activation Laboratories (Canada) after alkaline dissolution with lithium metaborate/tetraborate, followed by nitric acid dissolution. They were analysed according to Code 4Lithoresearch + Code 4BINAA analytical packages using Fusion-Inductively-Coupled Plasma (FUSICP). The obtained errors associated to reproducibility was in the order of 1

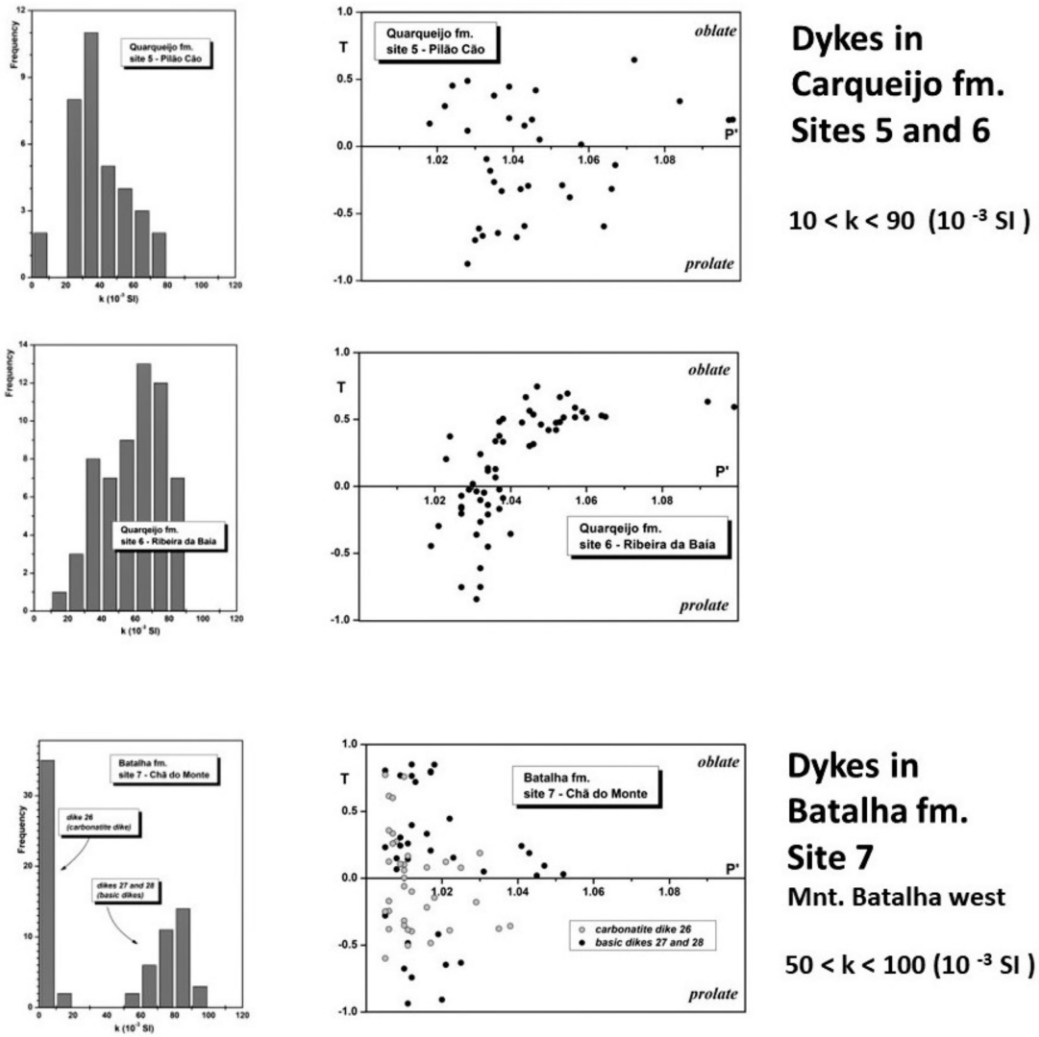

Figure 5b. Magnetic susceptibility distribution on dikes (left) and diagram of anisotropy degree P_J versus shape parameter T (right), sites 5, 6 and 7.

per cent. Detailed information on the analytical methods can be found at http://www.actlabs.com.

3.5 Dating dikes: $^{40}Ar/^{39}Ar$ geochronology

Ages were determined for six dike samples using the $^{40}Ar/^{39}Ar$ method at the Noble Gas Mass Spectrometry Laboratory, at the Oregon State University (USA), after irradiation in the TRIGA reactor with neutrons at 1 MW power for 6 h along with the FCT-3 biotite standard (28.03 ± 0.01 Ma age) to monitor the neutron flux.

$^{40}Ar/^{39}Ar$ analyses were performed using a MAP 215–50 rare gas mass spectrometer. Argon extraction by incremental step heating was achieved for groundmass with a Merchantek 10-Watt continuous fire CO_2 laser. Samples were degassed during 10 to 16 temperature steps, depending on individual sample characteristics, from 400 to 1400 °C. Prior to age calculation, all data were corrected for system blanks, mass fractionation and interfering argon isotopes generated by Ca, K and Cl during irradiation.

The $^{40}Ar/^{39}Ar$ ages of the studied samples were calculated using the ArArCALC v2.2 software package (Koppers 2002). The decay constant used throughout the step age calculation was $\lambda = (5.530 \pm 0.097) \times 10^{-10}$ a^{-1}, the corrected value of Steiger & Jäger (1977) reported by Min *et al.* (2000). The initial Ar composition was assumed to be atmospheric ($^{40}Ar/^{39}Ar = 295.5$) for plateau calculations.

4 SITE CHARACTERIZATION AND DIKE SAMPLING

An initial field survey provided the location of the main areas of Maio presenting dike swarms. From this initial survey we chose 7 representative sites in three of the major geological units dated from the Lower Cretaceous to the Miocene (Fig. 2 and Table 1). In the southern part of the island, we selected two sites in Ribeira de Cumiassa, in the Miocene Casas Velhas fm. and another two in Dom João bay area, in the Lower Cretaceous Batalha fm. East of the CIC two sites were chosen, one at Pilão Cão and another at Ribeira da Baía, in the Lower Cretaceous Carqueijo fm. Finally, another site at Chão do Monte, west of the CIC, also in the Batalha fm.

We identified and measured the attitude of 290 planar intrusions, formed by hypabyssal rocks, usually porphyritic, with phenocrysts of clinopyroxene and/or olivine set on an aphanitic groundmass.

From these sites, 27 dikes (26 mafic and one carbonatitic) were sampled for magnetic study (Fig. 2 and Table 1).

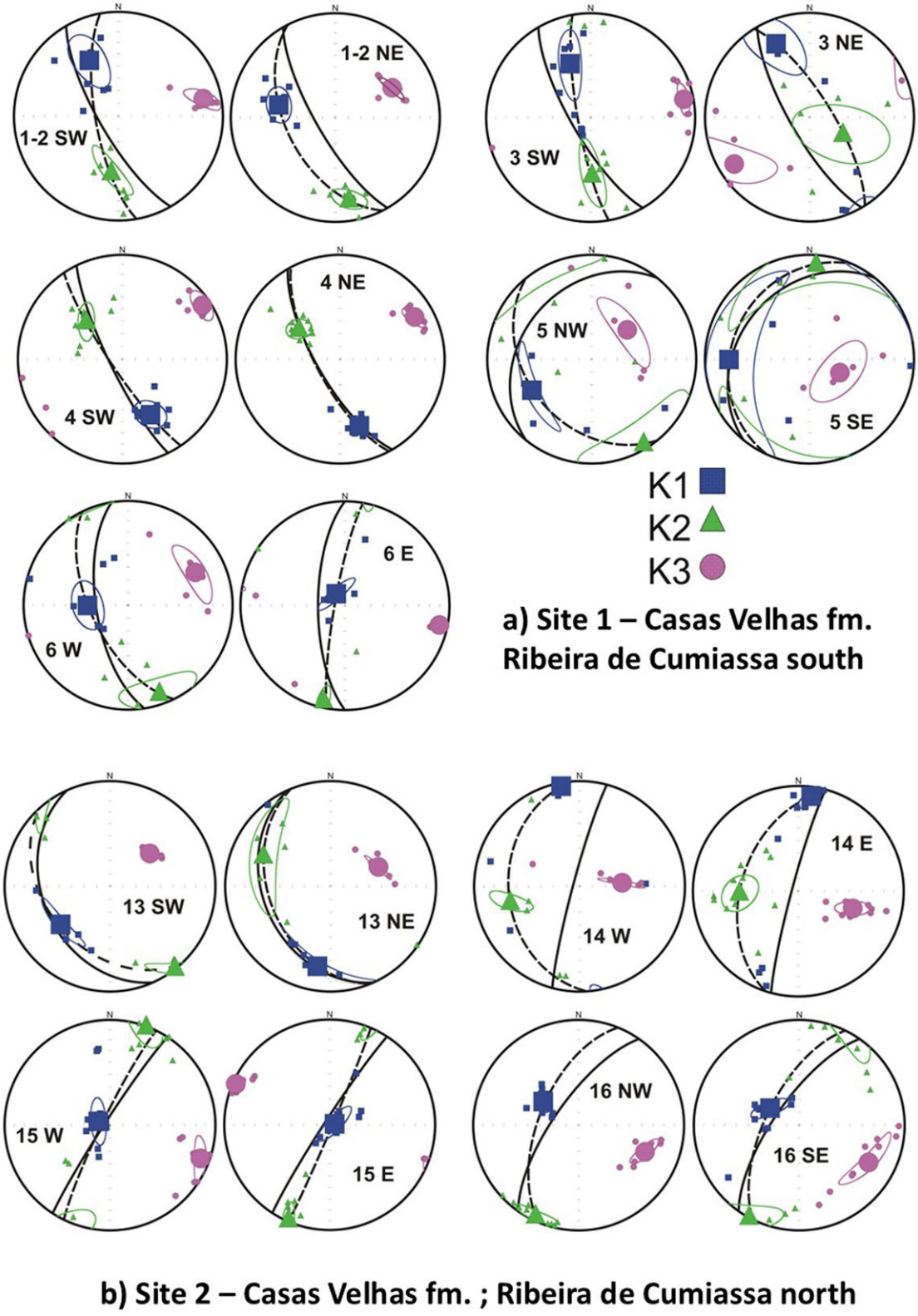

Figure 6a. Sites 1 and 2–Lower hemisphere, equal area projection of principal susceptibilities k_1 (squares), k_2 (triangles) and k_3 (circles), respectively, the maximum, intermediate and minimum susceptibilities at both margins of all dikes. Mean directions and confidence ellipses are represented. Solid line represents the mean plane of dike margin, hatched line represents magnetic foliation plane. The 95 per cent confidence ellipses were calculated from Jelinek statistics using the Anisoft' software from Agico. (https://agico.cz/text/software/anisoft/anisoft.php).

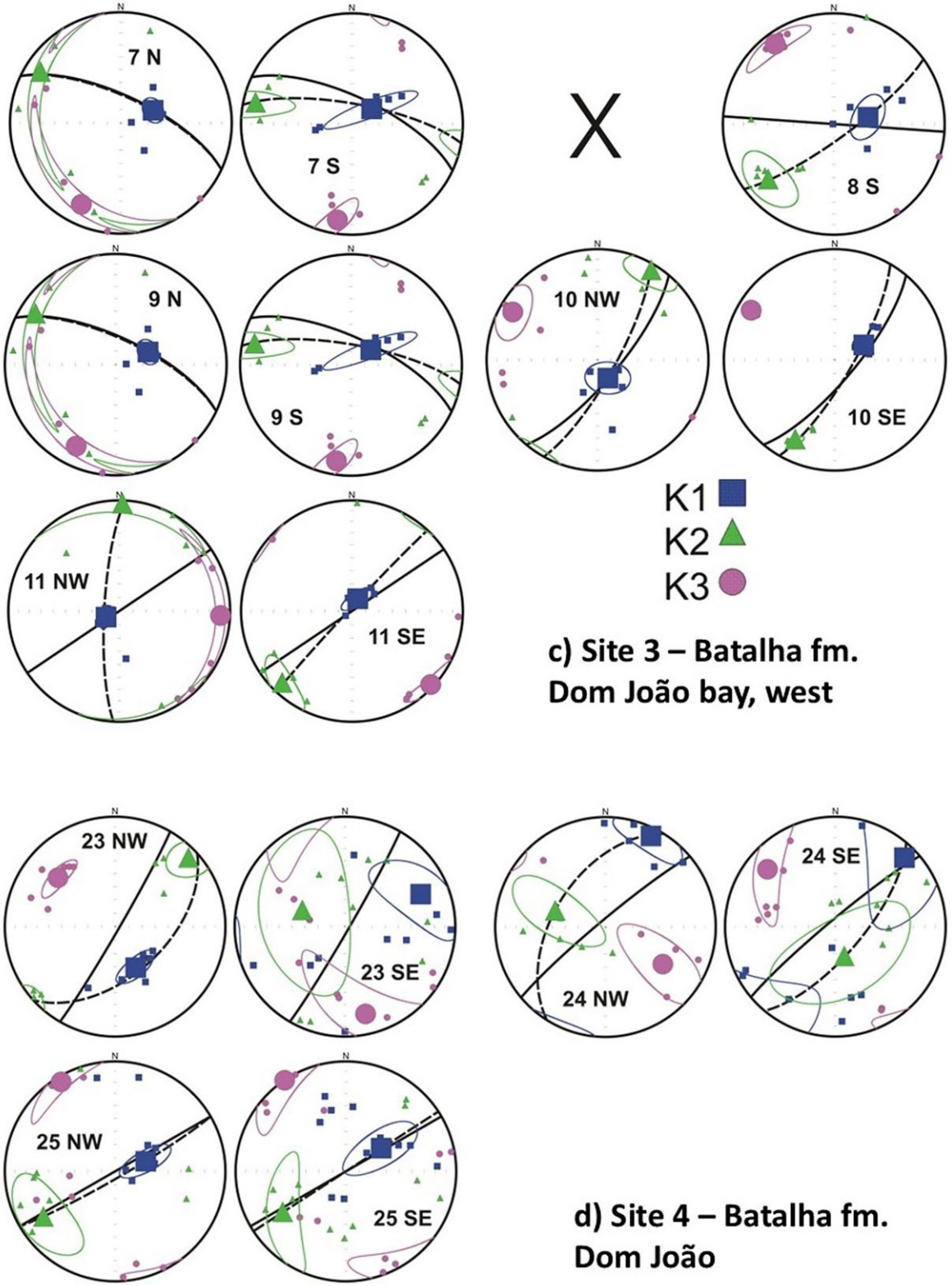

Figure 6b. Sites 3 and 4 (see previous caption).

The sampled dikes are vertical to subvertical, dipping more than 75º with widths ranging between 0.5 m to a maximum of 4.0 m. In general, the rock is strongly fractured with various degrees of weathering but, whenever possible, samples were collected, as fresh as possible, in both chilled margins (Fig. 3). The average orientation of the dike and orientation of the margin, close to each sampled core or sampling section, were systematically measured. From the 27 selected dikes we collect a total of 272 oriented cores from which 424 cylindrical specimens of the standard dimensions (25, 4 × 22 mm) were obtained.

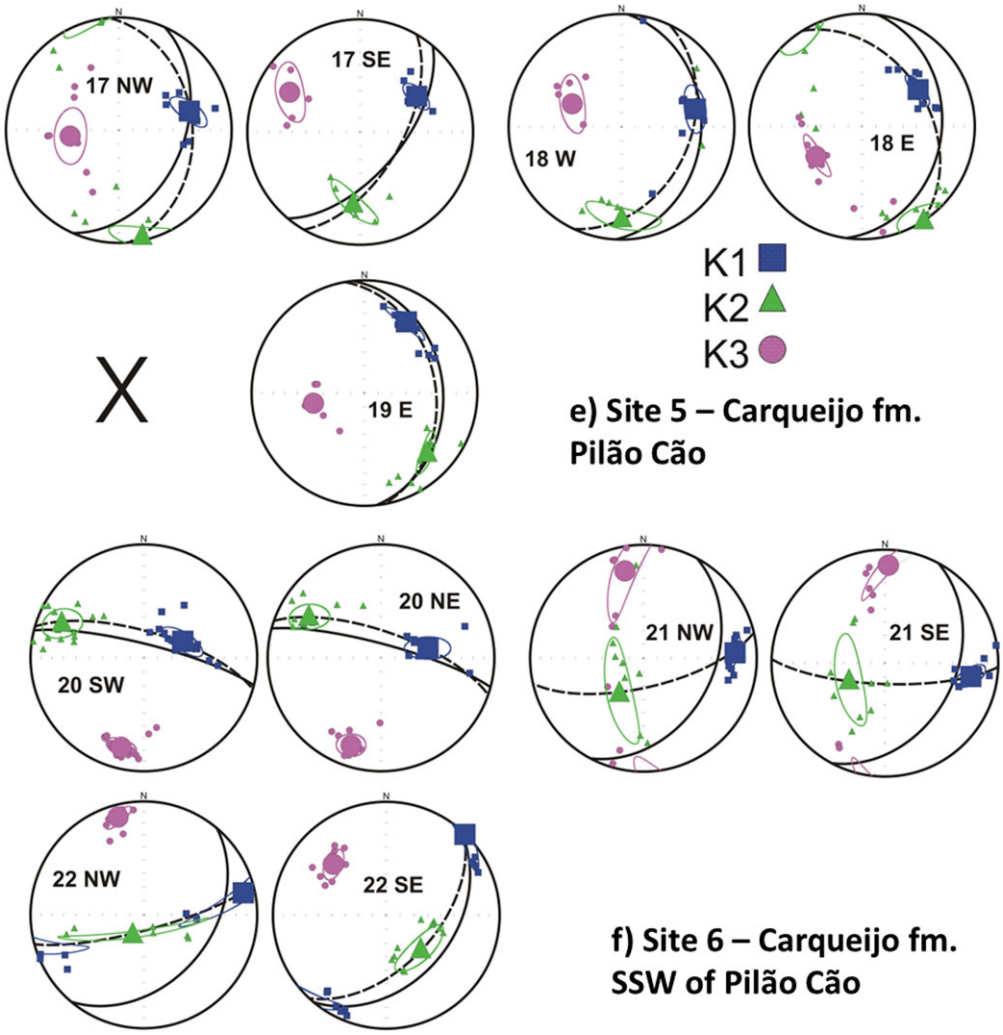

Figure 6c. Sites 5, 6 and 7 (see previous caption).

In the sites 1 and 2 of Casas Velhas fm. we measured the attitude of 56 dikes cutting through hyaloclastites and pillow lavas. Most dikes present dips steeper than 60° to the western quadrants. Their directions vary between NW–SE and NE–SW.

In sites 3 and 4, we measured 103 intrusions cutting through the MORB pillows of Batalha fm. The density of dikes and sills in those locations is so high that the intruded formations are almost completely obliterated. Most intrusions (98 per cent) are steeper than 60°.

In site 5, we identified 13 intrusions cutting through the Carqueijo fm., 12 of which present shallow dips ($30^o < I < 60^o$). In site 6 (also Carqueijo fm.) we measured 37 intrusions showing two typical distributions: 21 intrusions show dips $> 60^o$ while the remaining 16 show dips between 60^o and 30^o. In site 7, in the Batalha fm., we measured 29 intrusions, 24 of them dipping $> 60^o$.

5 RESULTS

5.1 Lithological characterization

The dikes sampled for this study are mostly silicate rocks but also included one thick (≈4 m) carbonatite dike. Representative major element analyses of the studied dikes are presented in Table S1, Supplementary Material S1. As can be seen from this table, most of the silicate rocks are characterized by somewhat high "Loss on Ignition", LOI (>3 per cent) mostly due to alteration. Consequently, the following considerations must be regarded with caution.

Most of the analysed silicate rocks are characterized, even on a volatile-free basis, by SiO_2 contents lower than 45 wt. per cent, which allow its characterization as ultrabasic, in the sense of IUGS (International Union of Geological Sciences; e.g. Le Bas *et al.* 1986). The exceptions are the dikes Ma17 and Ma22 (both in Carqueijo fm.) which have silica contents slightly higher than this threshold value (46.95 and 45.28 per cent, respectively), thus classifying as basic. All samples are alkaline being characterized by $(Na_2O + K_2O)/SiO_2$ ratios higher than 5 (up to 12.68), on a volatile-free basis. Except for sample Ma17, all the silicate samples plot on the tephrite/basanite field of the TAS diagram (Le Bas *et al.* 1986). Considering the calculated olivine normative contents, they are classified as tephrites, with exception of samples Ma27 and Ma29 which owing the normative olivine higher than 10 per cent are considered basanites. The most evolved sample (Ma17) plot as a phonotephrite, while sample Ma15 plot as a foidite (Table S1 and Fig. S1, Supplementary Material S1). As is typical of alkaline rocks, all samples are silica-undersaturated as depicted by normative compositions with $ne + lc$ ranging from 4.36 per cent up to 19.51 per cent.

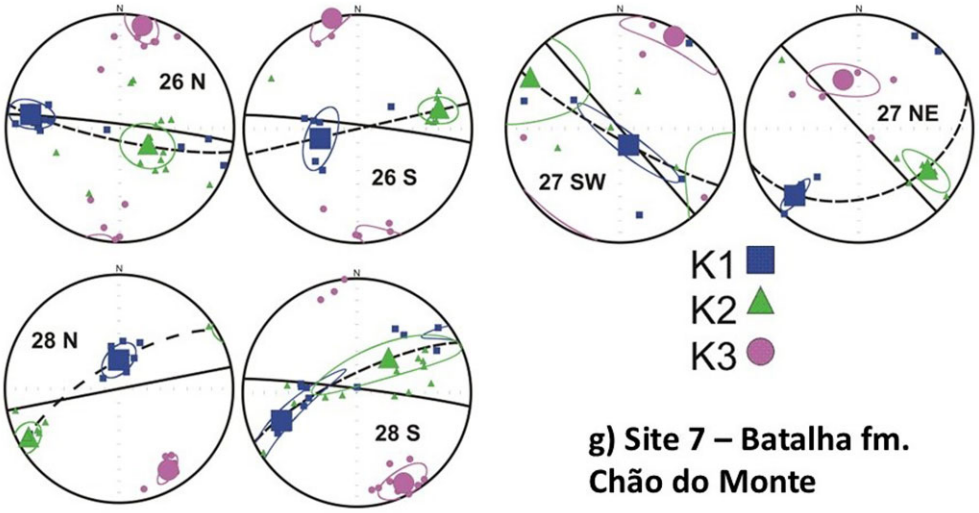

Figure 6d. Site 7 (see previous caption)

Most samples are porphyritic with aphanitic groundmass sometimes including glass (e.g. Ma7), which suggests high cooling rates and a final emplacement of these dikes at very shallow depths. Some samples have petrographic characteristics akin of lamprophyre rocks, with a phenocryst assemblage marked by the abundance of amphibole but lacking feldspars (Ma8 and Ma11 from Batalha fm.; Ma17 and Ma22 from Carqueijo fm.). Sample Ma22 shows amphiboles with evident signs of reaction with melt resulting in pervasive growth of oxides. The carbonatite dike (Ma26, Ma26A) is classified as a magnesiocarbonatite (Table S1 and Fig. S2, Supplementary Material S1).

5.2 $^{40}Ar/^{39}Ar$ dike age determinations

Step-heating incremental $^{40}Ar/^{39}Ar$ dating of six dikes range in age between 9.3 and 11.3 Ma. Two of them (Ma29 and Ma30), intruding the Morro fm, north of sites 5 and 6, were not studied for magnetic properties. Results are summarized in Table 2 and Fig. 4. Plateaux ages were retained for discussion, considering plateaux as sections of the age spectra encompassing 50 per cent or more of the total released ^{39}Ar in at least five consecutive heating steps with overlapping ages (Schaen *et al.* 2020).

To evaluate the obtained ages, statistical methods were applied. F statistics (Mean Square Weight Deviation—MSWD) and chi-square test are characterized by values significantly below 2.5 (MSWD) and p values clearly above 0.05, considered the threshold values for reliable ages (Baksi 2003, 2006; Ivanov *et al.* 2009; Norman *et al.* 2010; Schaen *et al.* 2020), thus producing indisputable plateau ages.

5.3 Magnetic susceptibility and anisotropy

The magnetic susceptibility (MS) of the mafic dikes ranges from 10×10^{-3} to 110×10^{-3} SI with a mean value of $k = 53 \pm 26 \times 10^{-3}$ SI. Data is presented on Table S2 in Supplementary Material S1.

Dikes from sites 1 and 2 (Fig. 5a) display low values of MS with mean $k = 32 \times 10^{-3}$ SI and very high values of anisotropy. The degree of anisotropy in site 1 is $P_J = 1.045 \pm 0.055$ increasing in site 2 to $P_J = 1.110 \pm 0.125$. Some samples in site 2 reach values of $P_J \approx 1.500$.

Dikes from sites 3 and 4 (Fig. 5a) display the largest range of susceptibilities with $10 < k < 110$ ($\times 10^3$) SI, suggesting higher differences in the amount of magnetic components. The anisotropy is low with $P_J < 1.060$.

The dikes from sites 5, 6 and 7 (Fig. 5b) show a narrower range of susceptibilities, with $20 < k < 80$ ($\times 10^3$) SI.

The carbonatite dike of site 7 (Fig. 5b) presents very low MS with a mean $k = 5.1 \pm 2.2 \times 10^{-3}$ SI, low anisotropy with $P_J = 1.015 \pm 0.006$ and an almost neutral shape of the ellipsoid with $T = -0.030$.

5.4 Magnetic fabric data and characteristics

The magnetic fabric and AMS from all dikes are represented in the stereoplots of Figs 6(a)–(d). Magnetic values and parameters are summarized in Table S2, Supplementary Material S1.

All dikes from sites 1 and 2 intruding Casas Velhas fm. (Fig. 6a) show normal magnetic fabric, mostly with a triaxial distribution of axes (confidence ellipses small and not overlapping); some dikes show an oblate magnetic fabric (confidence ellipses for mean k_1 and k_2 axes usually elongated and overlapping). Dikes 1 to 3 show k_1 axes with intermediate to shallow inclination to the NW; dike 4 shows k_1 axes with shallow inclination to the SE and dike 6 shows k_1 vertical to subvertical axes. In site 2, the dikes with NE–SW orientation show predominantly vertical k_1 axes. Only the shallow dipping dike 13 shows k_1 with shallow to intermediate inclination to the SE.

In sites 3 and 4 (Fig. 6b), the dikes are mostly vertical to subvertical with orientations varying from NE–SW to ESE–WNW. Despite the multiple dike orientations, the most frequent magnetic fabric is normal. In site 5 (Fig. 6c), dike 17 trending NNE–SSE and dikes 18 and 19 trending N–S present a shallow inclination ($20° < I < 30°$) to the east. Despite these differences they all show normal magnetic fabric with magnetic lineation systematically oriented to the E or NE, roughly along dip.

In site 6 (Fig. 6c), two dikes (21 and 22) show N–S and NNE–SSE orientation, similar to the dikes of site 5, with shallow inclination ($20° < I < 30°$) to the east. In dike 21, the k_1 and k_3 axes are almost parallel to the dike with k_2 axis closer to the dike pole.

Dike 20 shows a very distinct ESE–WNW subvertical attitude, different from the remaining dikes. The magnetic fabric is normal, strongly triaxial with steep magnetic lineation, $I > 70°$, slightly dipping to the east in both margins.

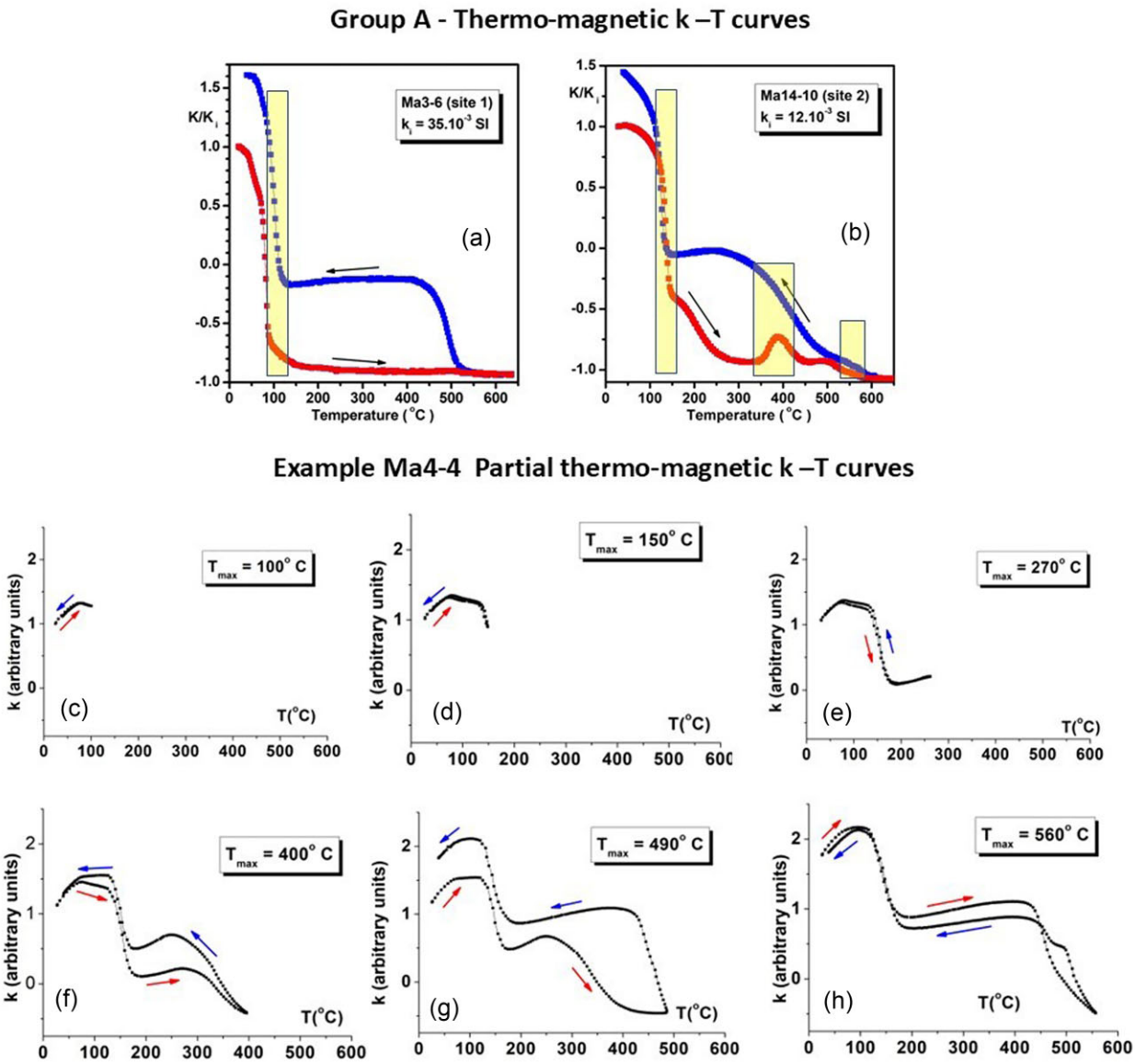

Figure 7. Representative $k(T)$ curves of the of the thermomagnetic behaviour of group A samples (7a and 7b) and a representative partial thermomagnetic k(T) cycle for Ma4_4.

In site 7 (Fig. 6d), the dikes 26 and 28 trend nearly E–W, while dike 27 is oriented NW–SE. All these dikes show normal magnetic fabric (MFP), except for the SW margin of dike 27, with inverse magnetic fabric. All the margins have a vertical to sub vertical k_1 axis, except for the N margin of the carbonatite dike 26 with a horizontal k_1 axis. Dike 28 shows imbrication of the MFP in both margins but in antisymmetric orientation.

5.5 Thermomagnetic $k(T)$ dependence curves

Continuous and partial thermo-magnetic cycles of low-field magnetic susceptibility were performed in 31 specimens from 16 selected dikes, including 26 from mafic rocks and five from the carbonatite rock with representative results depicted in Fig. 7 to Fig. 10.

Samples exhibit a wide variety of thermomagnetic behaviour. While some samples show a simple thermomagnetic behaviour characterized by a single magnetic phase, others show a complex evolution of magnetic susceptibility with two or three magnetic phases, and partial or totally different behaviour of the cooling and heating curves.

Based on the behaviour of the susceptibility dependence with temperature three different groups, here designed as A, B and C, can be distinguished:

Group A: the $k(T)$ curves show a low-temperature Curie point between 100 and 200 °C depending on the samples. With subsequent heating, the samples often show one intermediate Curie temperature in the 350 to 400 °C range, and then a final Curie temperature around 550 to 580 °C.

Up to 250−300 °C the partial thermo-magnetic curves are reversible confirming the nature of the first Curie temperature. Above the temperature of 350 °C a new phase with higher susceptibility is produced by the heating process and the cooling path is no longer reversible, at least up to 500 °C. Despite this irreversibility, after attaining the Curie temperature of 570–580 °C, the cooling curve regularly follows the heating curve and the final susceptibility, at room temperature is only slightly higher than the initial susceptibility.

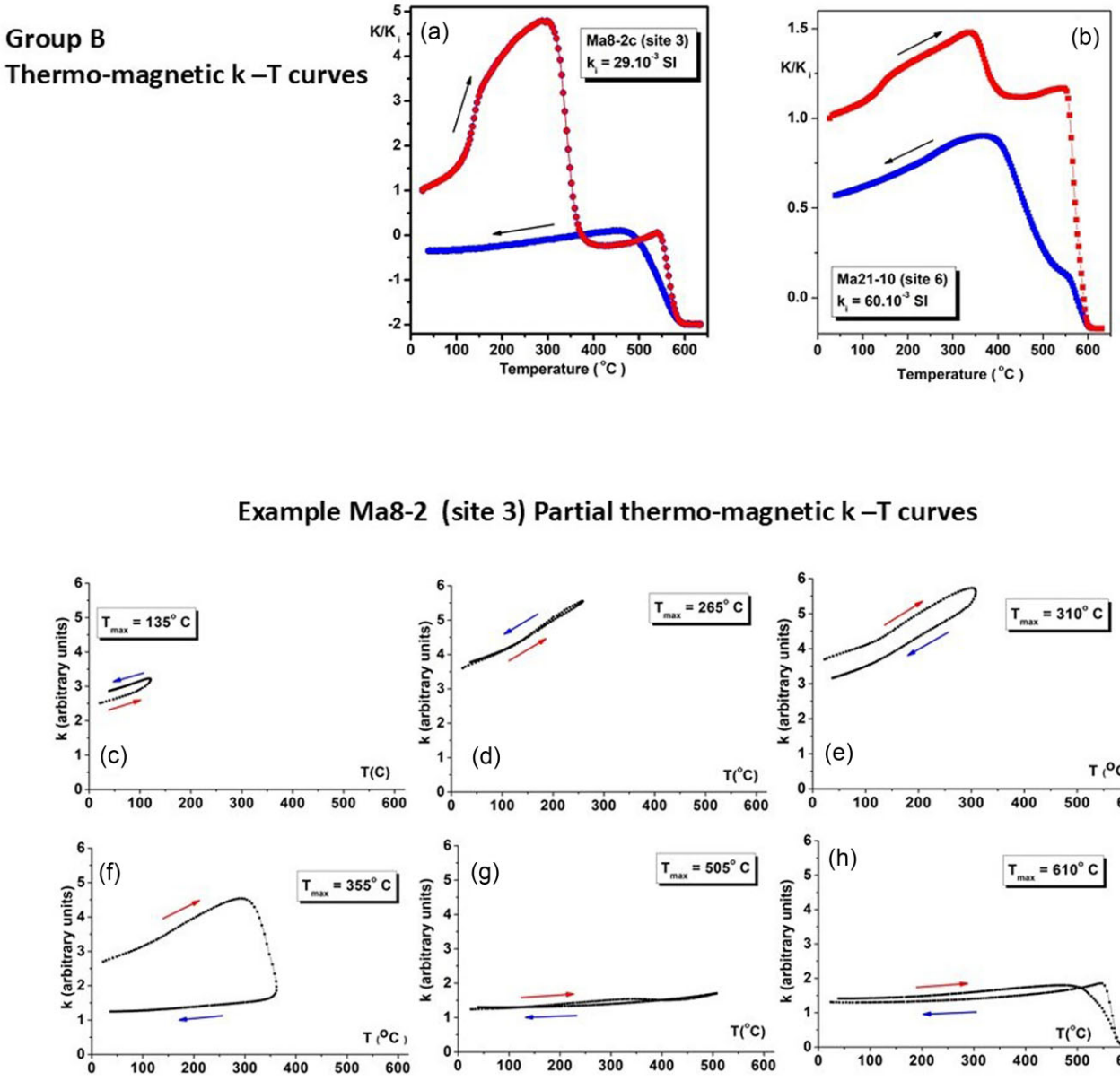

Figure 8. Representative $k(T)$ curves of the thermomagnetic behaviour of group B samples (Figs 8a to 8b) and a representative partial thermomagnetic $k(T)$ cycle (Figs 8c to 8h) for Ma8_2.

This low Curie temperature (100–200 °C) and the final ≈580 °C characterizes a Ti-rich titanomagnetite. Some examples also show vestiges of an intermediate Curie temperature at 350–400 °C. The gradual decrease in magnetic susceptibility (MS) from 500 to 580 °C—rather than a sharp drop at 570–580 °C—further supports the presence of a titanomagnetite solid solution with significant titanium content, which tends to reduce the Curie temperature of magnetite. Only samples from Casas Velhas Fm. (sites 1 and 2) show this characteristic thermo-magnetic behaviour.

Group B: The *k–T* curves show a continuous, but irregular, increment of MS, reaching a kind of 'shoulder' followed by a rapid decrease of the MS around 350 to 400 °C. With increasing temperature and reaching 560–580 °C a final sharp decrease of the MS occurs, clearly defining a Curie temperature of magnetite. The cooling curve follows a different path, with a final MS usually lower than the initial MS at room temperature.

The thermomagnetic curves (see Ma8-2 from site 3 in Figs 8e–j) show reversibility up to a temperature ≈ 300–330 °C. After this temperature a new magnetic phase with lower susceptibility occurs and after 350 °C the irreversibility is obvious (see Fig. 8h) indicating magnetic alteration of the maghemite (maghemite inversion).

The new magnetic phase obtained after the 350–400 °C temperature shows a very well-defined Curie temperature and perfectly reversible cooling path,

Group C (Fig. 9) is characterized by samples displaying two magnetic phases: a dominant major phase with a Curie temperature between 580 and 590 °C and evidence of a magnetic phase with Curie temperature in the range of 300–400 °C suggesting the presence of a small amount of titanomaghemite.

The carbonatite samples (Fig. 10) show a dominant magnetic component, revealed by Curie temperature around 575–585 °C and

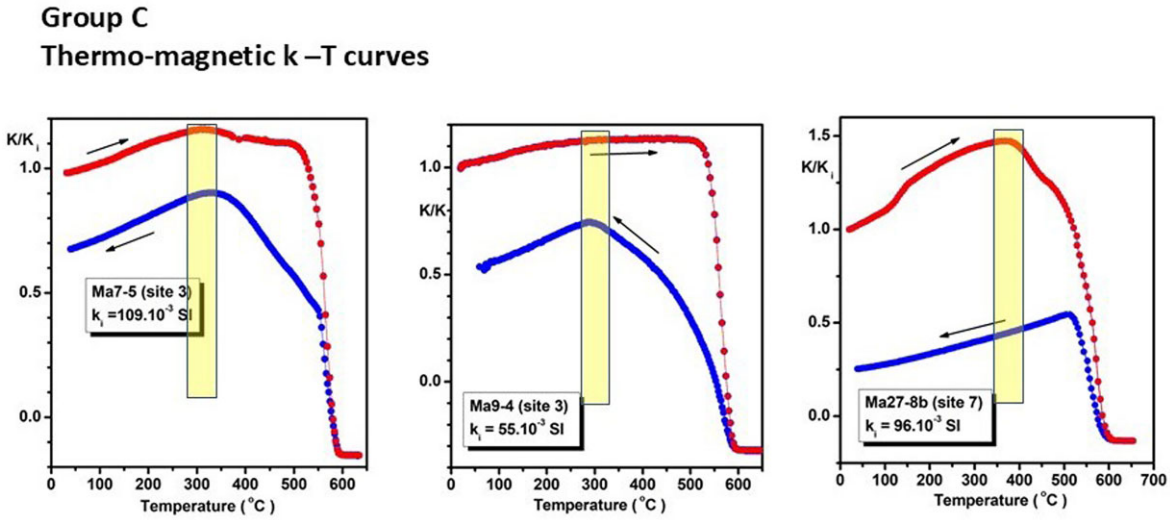

Figure 9. Representative $k(T)$ curves of the of thermomagnetic behaviour of group C samples.

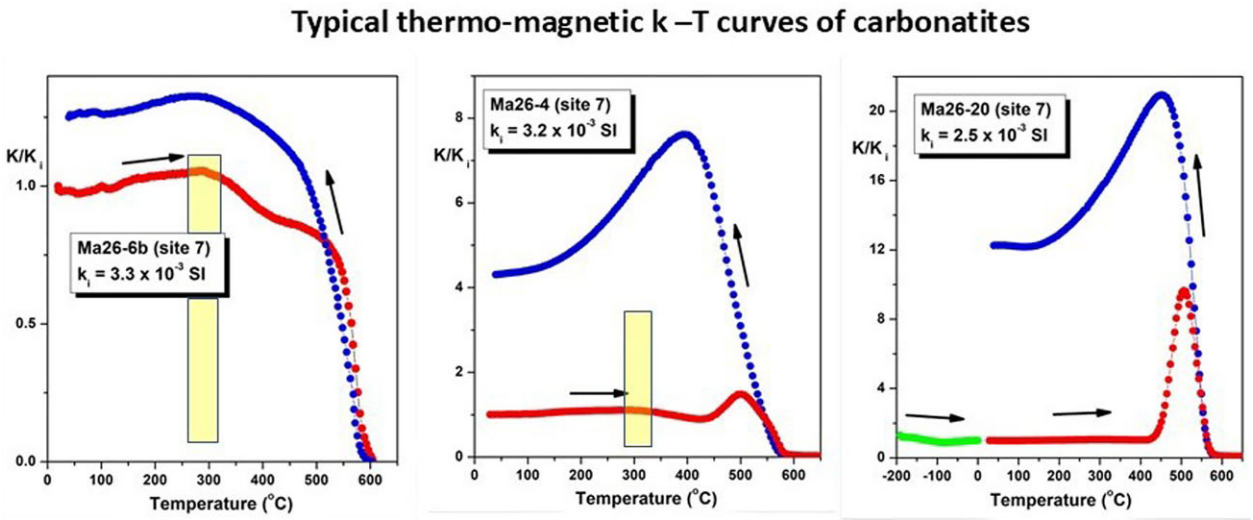

Figure 10. Representative $k(T)$ curves of the of thermomagnetic behaviour of carbonatite samples from dike 26.

a small kink usually observed at temperatures of ≈300 °C. A soft Hopkinson peak is also observed in some samples (see Ma26-4). This behaviour is observed in samples from dikes intruding the Batalha Fm. in sites 3 and 4 and in dikes from site 7 in the central-west part of the island (e.g. Ma7-5, Ma09-4, Ma27-4b and Ma28-12).

5.6 Isothermal remanent magnetization acquisition

Uniaxial, Isothermal Remanent Magnetization (IRM) was induced in 26 specimens, selected from the 7 sites. Overall, more than 95 per cent of saturation of magnetization (SIRM) is attained in fields below 0.3 T. From 0.5 T to 1.1 T, there is practically no increase in the IRM and so the maximum observed remanent magnetization is considered the SIRM (Fig. 11). The coercivity of remanence (H_{CR}), measured from the backfield demagnetization ranges from 10 to 60 mT, showing the dominance of a low-coercivity phase.

The separation of magnetic components, modelled by the Kruiver *et al.* (2001) method and represented in the LAP and GAP plots (Fig. 12), shows that most samples yield a bimodal coercivity spectra. In most cases an intermediate coercivity component is observed ranging from 25 to 90 mT along with a low coercivity component. Some samples show, with the characteristic intermediate coercivity component, a higher coercivity component but never exceeding 200 mT. A few samples show a coercivity described by a single component usually of intermediate coercivity. The intermediate coercivity component is, by far, the most representative of the coercivity spectra of these rocks.

6 DISCUSSION

6.1 . Geochronological constraints

The rocks cropping out at Maio Island comprise uplifted Early Cretaceous oceanic crust (MORB pillow lavas and hyaloclastites and deep-sea sediments) intruded and overlain by alkaline Miocene rocks (Samrock *et al.* 2022 and references therein). Previous K–Ar dating for Miocene dike intrusions in Batalha fm., Morro fm. and Carqueijo fm. (Mitchell *et al.* 1983), show that the age of the dikes ranges from 15.4 ± 0.3 Ma to 8.1 ± 0.6 Ma, with a major period

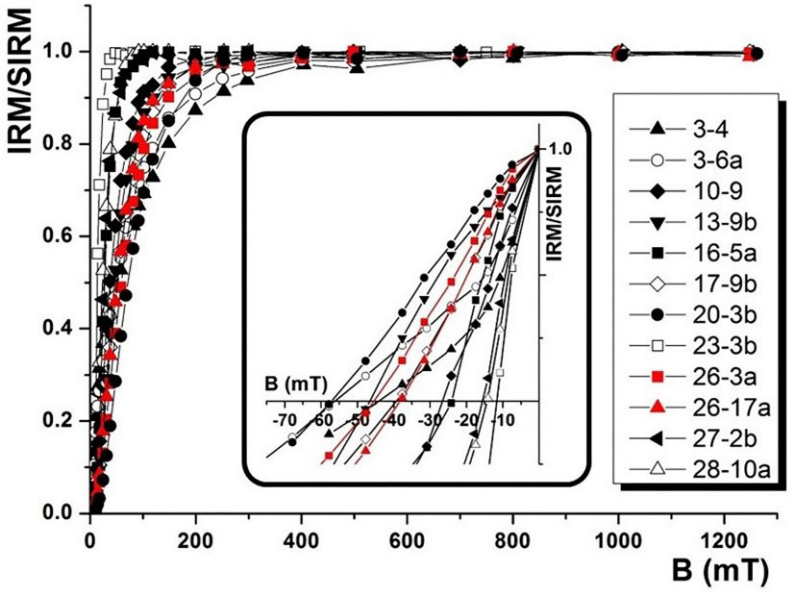

Figure 11. Isothermal remanence acquisition normalized to SIRM, for selected samples.

of dike intrusion around 11 Ma. Recently, Samrock *et al.* (2022) combined the previous K/Ar ages with their new $^{40}Ar/^{39}Ar$ and suggest three phases of intrusive activity and correspondingly high-volcanic activity in Maio: a first one recorded in dikes intruding the CIC and Coruja fm., from ∼16 to 13.5 Ma, a second one recorded in dikes that intruded the CIC, the Batalha fm. and Carqueijo fm., from ∼12 to 10 Ma, and a third one recorded mainly in dikes that intrude Morro fm., from ∼9.5 to 8 Ma, but with the second and third phases showing a slight time overlap.

In this study, we obtained $^{40}Ar/^{39}Ar$ ages spanning from ≈11.3 Ma to ≈9.2 Ma (see Fig. 13 and Table 2).

These results show that all the dated dikes are related to the Miocene island building phase (Tortonian age), and not contemporaneous with the Early Cretaceous ocean-floor volcanism nor the initial stages of the CIC formation, attributed to the Paleogene (∼19 Ma; Mitchell *et al.* 1983) and considered the most ancient alkaline rocks cropping out on the island.

None of the dikes dated in our study is integrable in the first phase defined by Samrock *et al.* (2022), with all of them being assignable to the 2nd and 3rd phases of these authors, yet with somewhat distinct distribution. It is the case of the age of 9.34 ± 0.07 Ma determined for sample Ma20 intruded into the Carqueijo fm. and the age of 10.18 ± 0.12 Ma obtained for a sample (Ma30) intruding the Morro fm. The age obtained for a dike intruding the Batalha fm. is within the range of previously obtained ages by Mitchell *et al.* (1983) and Samrock *et al.* (2022) (see Fig. 13), being slightly older than the values obtained by the last authors. However, our results expand the range of dike intrusions ages into the Morro fm. to as old as 10.18 ± 0.12 Ma, and to ages as young as 9.34 ± 0.07Ma at Carqueijo fm. (see Fig. 4). We also obtained the first reported age for a dike intruding the Casas Velhas fm. (≈9.2 Ma).

6.2 The link between mineralogy and whole-rock compositions

The studied rocks have TiO_2 contents as high as 4.79 wt. per cent. However, from the previous discussion (see Section 5.5) it can be inferred that primary ilmenite ($FeTiO_3$), is very scarce or even absent as primary mineral, among the oxide minerals in the studied dikes. This is not surprising given the highly silica undersaturated (normative $ne + lc$ up to 19.51 per cent) composition of these dikes. Indeed, it has been shown that the low SiO_2 activity favours the Ti incorporation in clinopyroxenes, thus inhibiting the later generation of ilmenite (e.g. Carmichael *et al.* 1974; Mata & Munhá 2004).

On the other hand, the Ti-rich titanomagnetites rocks (Group A previously defined in Section 5.5, showing a characteristic magnetic phase of low Curie temperature) are those, also characterized, by TiO_2 contents higher than 4.30 wt. per cent (up to 4.79 wt. per cent) found in sites 1 and 2, as opposed to rocks from sites 3, 5, 6 and 7 for which TiO_2 concentrations are below 4.30 wt. per cent (down to 3.32 wt. per cent).

For the carbonatite dike the $k(T)$ dependence curves point to the dominance of magnetite, which agrees with the very low TiO_2 of this rock (0.11 wt. per cent).

6.3 Magnetic fabric and mineral preferred orientation

The use of AMS to study magma flow in dikes was historically first applied by Khan (1962), followed by Symons (1975) and Ellwood (1978). The observation of the orientation of the elongated vesicles at the margins of the dikes and the imbrication of clusters of the magnetic lineation k_1, in each margin and symmetrically arranged relative to the middle of the dike, was revealed by Knight & Walker (1988).

Indeed, the magmatic flow fabric in a dike is controlled by the fabric of the early crystallized phenocrysts, usually rigid particles and elongated phenocrysts with high aspect ratios. The magma flow direction can be constrained with the analysis of the AMS from opposite margins. Assuming no relative movement of the dike walls, and a laminar flow near the margin, the flow induces a strain gradient regime characterized by simple shear that progressively changes to pure shear in the central part of the dike. The elongated phenocrysts will rotate and become stacked and imbricated between them and against the wall (Ildefonse *et al*. 1992; Arbaret *et*

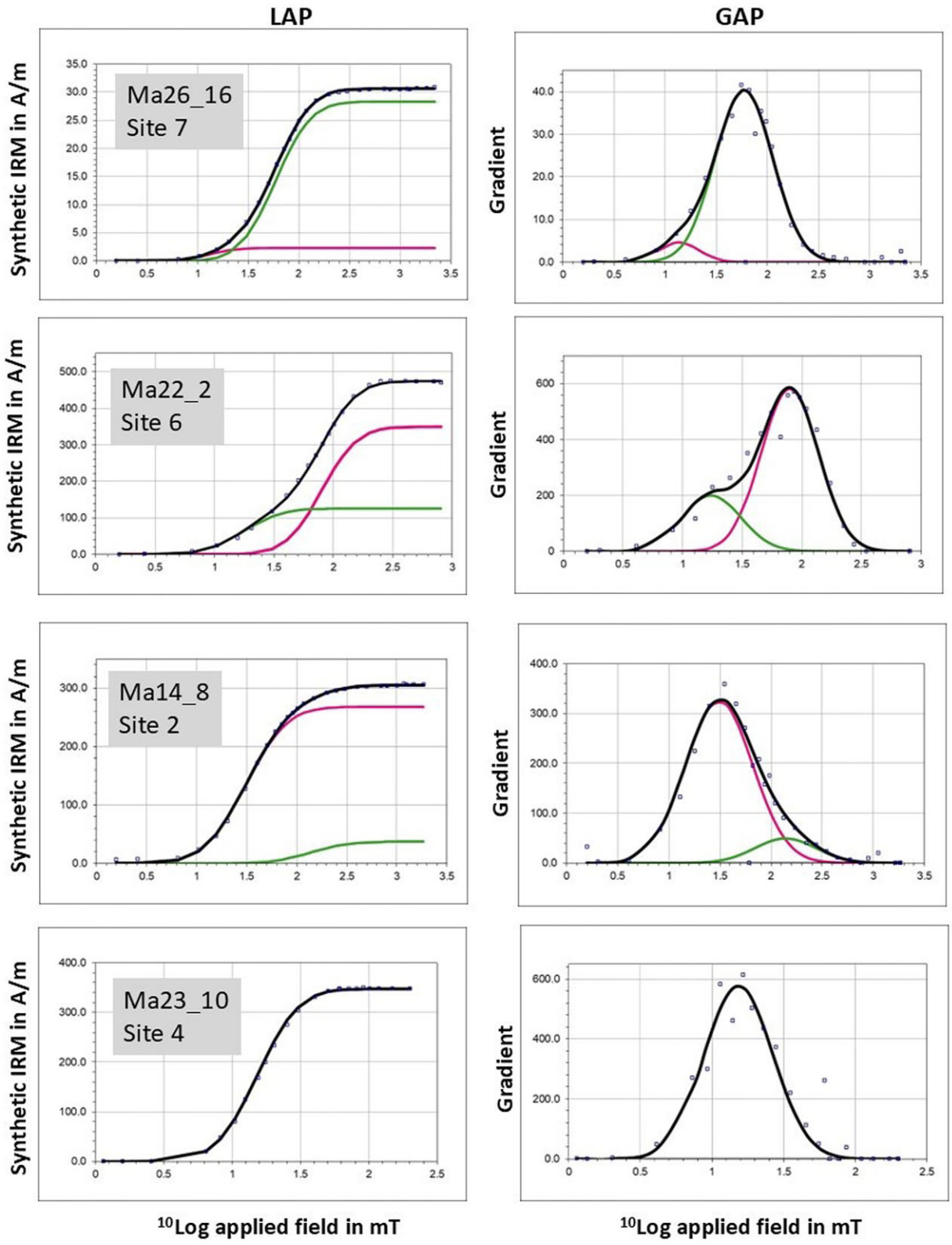

Figure 12. LAP and GAP diagrams for representative samples (see text for explanation).

al. 1996). This will determine that the long crystallographic axes of phenocrysts will be oriented making small angles to the dike margins, converging towards the magma source. For a dike emplaced with no wall-parallel shear during injection, in a pure extensional fracture, samples in opposing margins should show the magnetic fabric (or magnetic lineation or magnetic foliation plane) in a symmetrical imbrication (a small angle approximately between 10º to 30º in average, relative to the margins). This orientation allows an

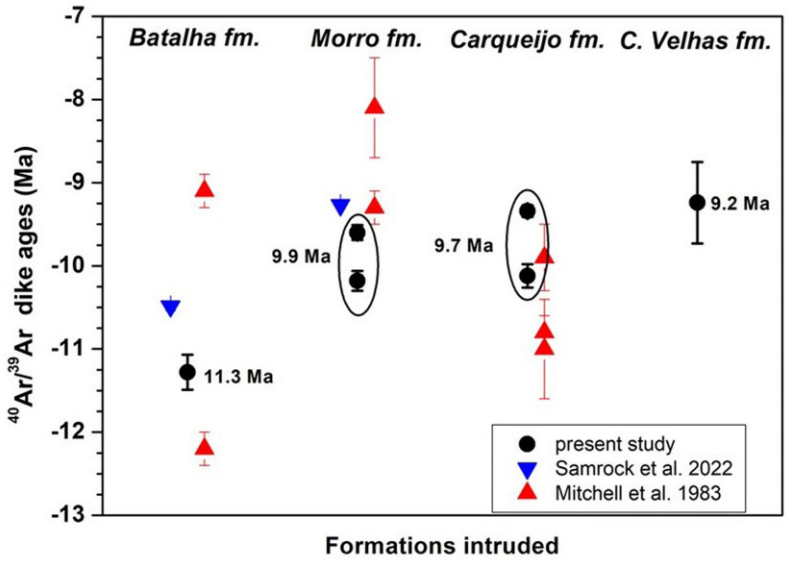

Figure 13. Compilation of K–Ar and $^{40}Ar/^{39}Ar$ ages of dikes from Maio Island from Mitchell *et al.* 1983 and Samrock *et al.* 2022, and the new ^{40}Ar–^{39}Ar ages obtained in this study. The 2σ errors are indicated by error bars. Data points encircled represented different ages from different dikes intruding the same formation. The obtained ages are indicated.

unambiguous magma flow direction and sense to be determined (Dragoni *et al.* 1997; Moreira *et al.* 1999, 2015; Geoffroy *et al.* 2002, 2007; Callot & Guichet 2003; Philpotts & Philpotts 2007; Silva *et al.* 2014; Warwick *et al.* 2014). If the intrusion is contemporaneous with a lateral, along strike displacement in the margins, the fabric in each margin should show an antisymmetric orientation.

Indeed, the magnetic fabric of Maio dikes shows neither imbrication of the magnetic lineation, nor imbrication of the magnetic foliation plane. In the few margins in which it is possible to see a very subtle imbrication, it is so small and of the order of the angular confidence of the *k*3 axis, that it is not reliable the application of the imbrication model as used by Geoffroy *et al.* (2002, 2007), Callot & Guichet (2003) or Moreira *et al.* (1999, 2015) to deduce a direction for the magmatic flow.

To obtain a not-arbitrary choice between the magnetic axis (k_1 or k_2) as the proxy for the direction of the magmatic flow (magmatic fabric) a micro-textural optical analysis was performed. The objective was to determine the geometrical/structural relationship between preferred orientations (PO) of phenocrysts and the opaque (mostly Fe and Ti oxide) grains with the magnetic (AMS) orientations.

We chose samples from dikes with only normal magnetic fabric, discarding samples with mixtures of fabrics (inverse, intermediate, or abnormal magnetic fabrics) as well as samples from margins that show mixtures of oblate and prolate shapes. From this selection we found five dikes from sites 1 and 3 intruding two different formations from where thin sections were cut parallel to the magnetic foliation plane. From these thin sections, around 40 digitized microphotographs from optical microscopy were obtained.

For each microphotograph, we produced by image treatment two grey scale images, one of the filtered phenocrysts and another of the filtered opaques.

The quantitative analysis of preferred orientations of opaques and phenocrysts was made through the 'Intercepts' software (Launeau & Robin 1996) which uses a Fourier analysis to determine the boundary orientations of a specific mineral. The results were then compared with the orientation of the magnetic axes k_1 and k_2. The coherence between the directional Intercepts and AMS results was semiquantitatively evaluated by the R parameter—the shape fabric anisotropy obtained by the Intercepts algorithm in the opaque phase images—obtaining values regularly similar. Whenever possible, from each image the analysis of both phenocrysts and opaques was made. In some images, this was not possible as one of the phases (opaques or phenocrysts) were poorly defined. In these situations, we have results for only one phase. We estimate a maximum accumulated error of 10° in the comparison of directions, generated by the hand-made procedure sequence of marking the k_1 or k_2 directions in the specimen, cutting the thin section parallel to the k_1–k_2 plane, and transport these magnetic directions into the thin section. The obtained analysis and results are summarized in Table S3 in Supplementary Material S1 and three selected samples are exemplified in Fig. 14. Full results are summarized and graphically represented in Fig. 15. The analysis of PO of phenocrysts versus k_1 orientation shows an almost mono-modal correlation. The angular difference is lower than 15° in 56 per cent of the analysed images and lower than 30° in 70 per cent of the images. The analysis of PO from opaque grains versus the k_1 orientation shows that, in most images, the PO of the oxides is coaxial with the k_1 direction (in 45 per cent of the images the angular difference between both directions is $< 15°$ and in 58 per cent is less than 30°). In some images representing 26 per cent of total images analysed, the angle between k_1 and the PO of the oxides is greater than 75°.

We remark that, except for dike 2 that presents a very high degree of anisotropy and a shape parameter that tends to be oblate with the increase of anisotropy, in all other samples the mean shape parameter tends to be near neutral. The most common magnetic fabric in all remaining dikes is triaxial and normal, elsewhere.

Considering that the magnetic lineation predominantly present an alignment close to the PO of phenocrysts which is also close to the preferred orientation of the opaques and the lack of imbrication of the foliation plane relative to the margins, we concluded that the magnetic fabric is flow related and, at the scale of the dike/margin, the mean magnetic lineation is coaxial of the mean direction of the magmatic flow.

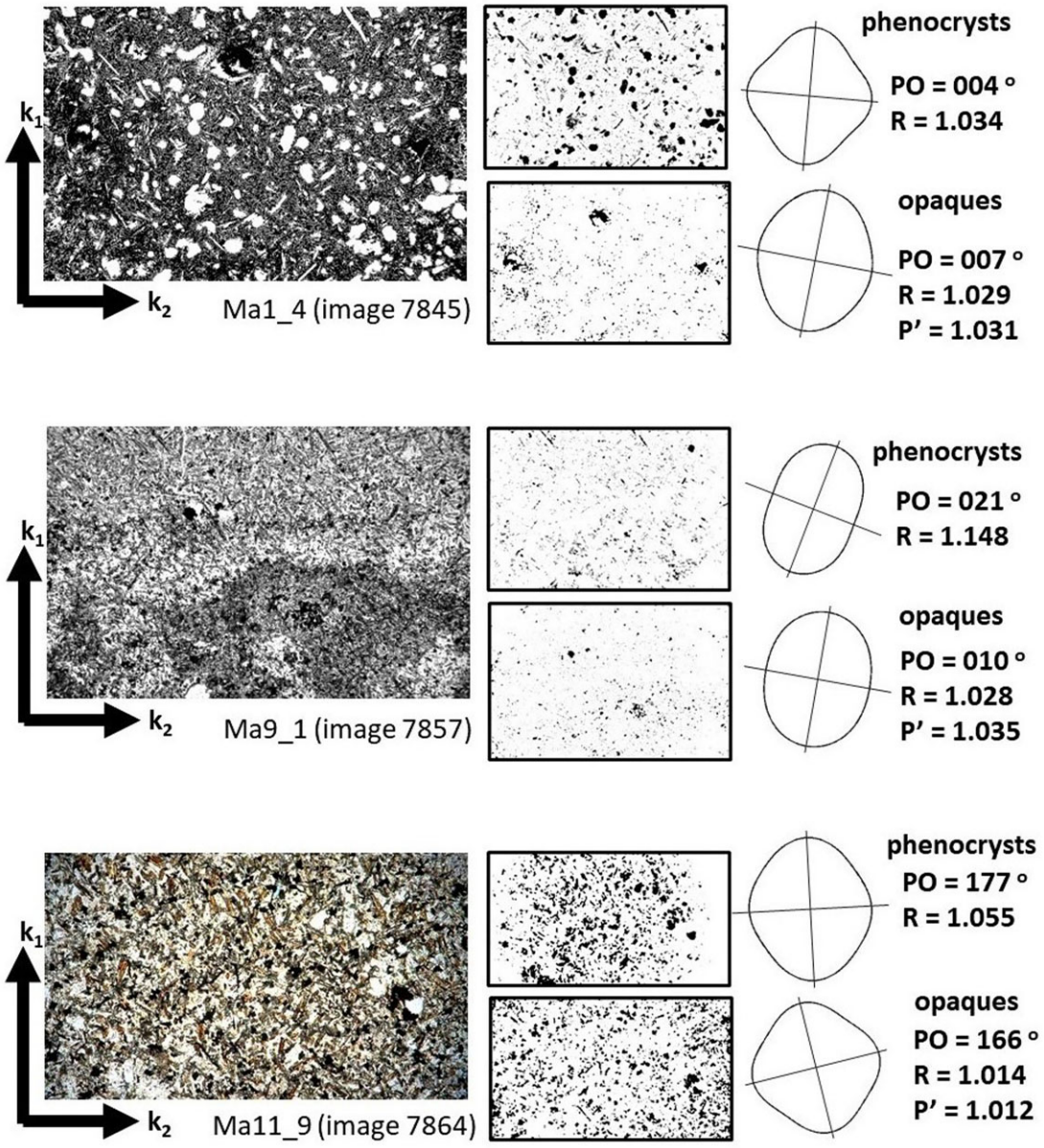

Figure 14. Selected examples of the analysis of the PO of phenocrysts and opaques in specimens Ma1-4, Ma9-1 and Ma11-9. For each specimen results are presented in three columns. Left column: image of the thin section with the magnetic axis's orientation. Centre column: the processed images for analysis after image improvement of the phenocrysts (above) and opaque (below). Right column: the resulting rose diagrams of orientations of phenocrysts (upper image) and opaques (lower image) obtained with 'Intercepts'. The PO obtained is specified in degrees relative to vertical axis (k_1) of image; *R* is the shape fabric anisotropy obtained from 'Intercepts'; P_j is the (AMS) degree of anisotropy. Note the good correlation of the *R* parameter (shape fabric from Intercepts) with the P_J parameter (magnetic anisotropy obtained from the AMS) in the opaques analyses.

6.4 Analysis of magnetic fabric and the deduced magma flow orientations

There are significant differences in the magnetic fabric and magnetic composition between the dikes at sites 1 and 2 which intrude into the Casas Velhas fm., and all other dikes.

Concerning the magnetic fabric the most evident points are the high-anisotropic magnetic fabric and the dominance of the oblate shape fabric that reveals a strong flattening strain effect.

It is well known that in rocks with dominant ferromagnetic (*s.l.*) grains, the magnetic fabric is attributed to three main processes: (1) domain anisotropy, (2) stress induced anisotropy and (3) shape anisotropy. For magnetite or titanomagnetite bearing rocks, especially with dominant multi-domain (MD) grains, which is the typical composition in these rocks, the prevailing effect is the shape anisotropy originated by alignment of magnetic grains (e.g. Stacey 1960; Kapicka 1983). Deformation (or anisotropy) and shape of the ellipsoid is mainly dependent on the stress that takes place during the emplacement and/or cooling of the magma.

The mean magnetic lineation is oblique in site 1 and turns to nearly vertical in dikes of site 2 where the magnetic anisotropy increases, and the oblate shape of the fabric becomes predominant. The increase of the magnetic anisotropy, already high in site 1 and

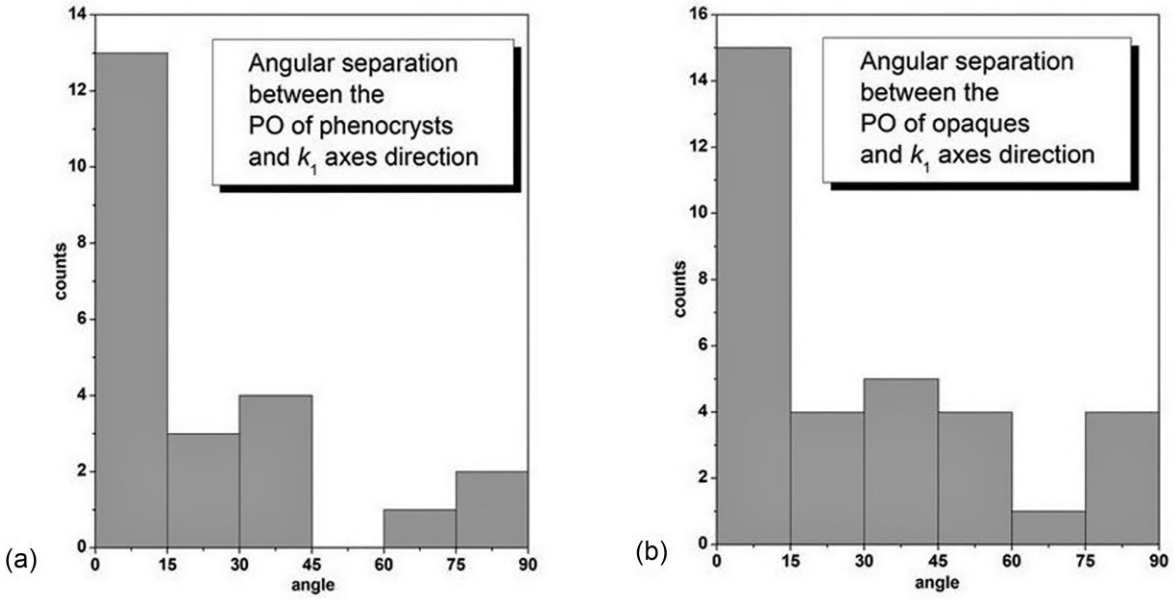

Figure 15. Histograms of the angular separation between preferred orientations (PO) of minerals and magnetic directions. (a) Left, measured angular differences between PO of phenocrysts, mainly plagioclases laths and magnetic lineation (k_1 axis). (b) Right, measured angular differences between PO of opaque grains (Fe and Ti oxide magnetic grains) and magnetic lineation (k_1 axis).

the dominant oblate shape, from dikes of sites 1 and 2, suggest that the magmatic source should be at very shallow depths where the intrusion pressure should be higher, and the direction of the flow should be mostly vertical.

Besides the differences previous discussed those dikes also show a dominant magnetic composition of Ti-rich titanomagnetite revealed in the thermomagnetic curves (chap. 5.5), concordant with the whole-rock composition (Section 6.1) of these rocks.

The dikes belonging to sites 3 and 4 (Fig. 16) intruding the oldest volcano-stratigraphic unit, the Batalha fm., despite the highly scattered attitudes, are roughly grouped into two major directions trending NE–SW and WNW–ESE. The magnetic mineralogy shows differences, but they are neither related with the site nor with their direction. Dikes from both sites show a composition dominated by Ti-poor titanomagnetite with different degrees of alteration and composition. Some samples show a complex multiphase composition, while others show a dominant (almost single) magnetite-like phase. These compositions are like those characteristics of samples that fall in the Group II (Ti-poor titanomagnetite with vestiges of titanomaghemite and probably ilmenite) and Group III (Ti-poor and dominant magnetite) which point to a variability and heterogeneity in the Fe and Ti oxides content.

These two sites show dikes with high heterogeneity of magnetic compositions. The Batalha fm. is the oldest unit exposed in Maio and thus it must be intruded by dikes of different magmatic phases and composition, resulting in significant variability in magnetic mineralogy.

Despite the differences in the magnetic mineralogy, the large range of dike orientations and the different shape of the magnetic fabric (dominantly triaxial in site 3, and dominantly prolate in site 4) the magnetic fabric is normal in these dikes. The magnetic lineation shows a uniform, almost vertical orientation, independently of the dike orientation or magnetic fabric, indicating a predominant vertical to subvertical magma flow orientation.

In sites 5 and 6, the N–S to NE–SW trending dikes intruding the Carqueijo Fm. display shallow to moderate dip values, dipping to the east. The magnetic fabric is always normal and triaxial. The magnetic lineation is well constrained and is usually coaxial with the dip direction of the dikes, with shallow to moderate inclination. The deduced magma flow orientation, coincident with the magnetic lineation, is in the dip direction, with a mean E–W orientation.

In site 6 the dikes, predominantly trending NE–SW, show magnetic lineation with a shallow inclination to the eastern quadrants. One dike with a different orientation, ESE–WNW, also displays a normal and triaxial magnetic fabric. The magnetic lineation is here oblique but also dipping eastwards.

In site 7, west of the CIC, one margin of dike 27 shows an inverse magnetic fabric, while the other margin displays a normal magnetic fabric, like the other two dikes sampled in this site. Both the carbonatite dike (Ma26) and the contiguous parallel mafic dike (Ma28) are subvertical with a mean E–W direction. They show magnetic lineation spanning from horizontal (in the N margin of dike 26), to steep, subvertical (in the north margin of dike 28). In dike 28, an imbrication of the MFP is observed in both margins. The imbrication shows an antisymmetric pattern relative to the dike axis, or a 'scissored' configuration that is compatible with an opposite, horizontal 'strike-slip' displacement of the dike margins in late stages of cooling.

This distinction may be related to different magmatic sources, which in this case favours the gravimetric model proposed by Represas *et al.* 2012, indicating the presence of two distinct plutonic bodies in the volcanic structure of the island. Indeed, one of the bodies would be located in the south of the island, near sites 1 and 2, were high values of magnetic fabric deformation and vertical magma flow were found, while the other would be located in the central and east part of the island feeding most of the intrusions southeast, east and west of the CIC.

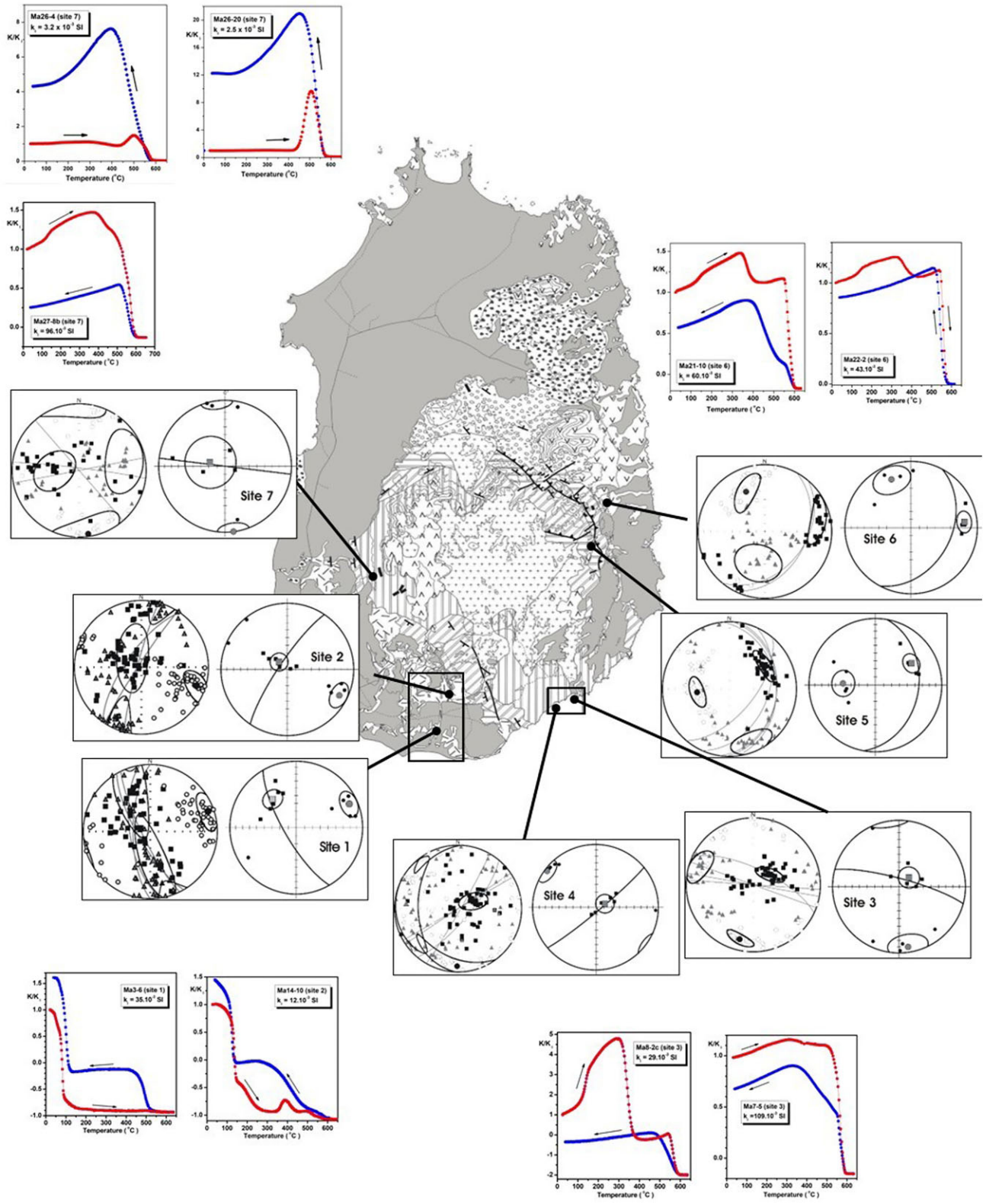

Figure16. Synthesis of AMS results for all studied dikes in Maio. For each site we show two stereoplots. The left stereoplot shows the AMS results (k_1, k_2 and k_3) in the real (field) orientation of the grouped dikes with similar attitudes (differences in direction and dip $< 20^o$). The right stereoplot represents the result of the rotation of the different dikes and mean magnetic directions (only k_1 and k_3) for a common referential. This referential is represented in the stereoplot by a 'synthetic' dike with the average orientation of the sampled dikes in that site. The corresponding magnetic axes of each dike were also rotated accordingly.

7 CONCLUDING REMARKS

The $^{40}Ar/^{39}Ar$ ages of the studied dikes of Maio Island range from 11.28 ± 0.21 Ma and 9.24 ± 0.49 Ma and enlarge the previous published age ranges for dikes intruding the Morro and Carqueijo fms. We obtained the first age for dikes intruding Casas Velhas fm. (9.24 ± 0.49 Ma).

From the k-T analysis, the dikes from Batalha and Carqueijo formations show a characteristic magnetic composition of Ti-poor titanomagnetite. However, differences in magnetic composition were observed. Some samples exhibited at least one additional magnetic phase, indicated by Curie temperatures ranging from 300 to 350 °C—interpreted as titanomaghemite (e.g. sites 3 and 4). In contrast, other samples showed a dominant single magnetite phase, with Curie temperatures around 570 to 585 °C and pronounced Hopkinson peaks (e.g. site 7), suggesting a significant contribution from single-domain particles.

Only the dikes from the Casas Velhas fm. display a characteristic and predominant Ti-rich titanomagnetite composition, occasionally accompanied by a minor intermediate magnetic phase with a Curie temperature around 400 °C. Dikes intruding the oldest formation (Batalha fm.) show the highest range of MS values between 10×10^{-3} SI to 110×10^{-3} SI, while all the remaining dikes show narrow range of MS values. The carbonatite dike presents, as expected, very low values of MS with $k < 10 \times 10^{-3}$ SI.

Magnetic fabric is normal with no imbrication to the margin. Numerical analysis of fabric leads us to consider that magnetic lineation is, therefore, the proxy of the magmatic flow axis direction. The magnetic anisotropy is usually low ($P' < 1.080$) except for the dikes of Casas Velhas fm. where the degree of anisotropy reaches very high values (P' reaching 1.5 in site 2)

The magnetic and geochemical differences observed between the Casas Velhas dikes, and all other dikes may be explained as being sourced from two distinct magma reservoirs located at different depths: a shallower, which explains the very high values of the magnetic fabric anisotropy and the inferred vertical magma flow observed in the Casas Velhas dikes, and a deeper source(s), located in a central position in the island, responsible for the dikes intruding the Batalha fm., Morro fm. and Carqueijo fm. The location of the youngest Casas Velhas dikes may also suggest a possible migration of the magmatic reservoir(s) from the central part of the island to the southwest. The magnetic and mineralogical differences and high heterogeneity of the Batalha fm. dikes may also be interpreted as resulting from a wider age range of the intrusions, compatible with the older age of Batalha fm. This diversity is also reflected in changes in stress field during dike emplacement (observed in the large range of orientations of the dikes intruding Batalha fm.) and different igneous mineral parageneses reflecting a large range of magmatic compositions.

ACKNOWLEDGMENTS

We would like to thank to Assistant Editor Fern Storey and reviewers Antonio Casas and Thor Hansteen for their valuable comments, which significantly enhanced the quality and the readability of the manuscript.

This work was supported by the Portuguese Fundação para a Ciência e Tecnologia, FCT, I.P./MCTES through national funds (PIDDAC): UID/50019/2025 and LA/P/0068/2020 https://doi.org/10.54499/LA/P/0068/2020). We acknowledge the Portuguese Fundação para a Ciência e a Tecnologia (FCT) I.P./MCTES through project CV-PLUME—an investigation on the geometry and deep signature of Cape Verde Mantle Plume (PTDC/CTE-GIN/64330/2006).

AUTHOR CONTRIBUTIONS

MM conceived the study. MM, JMata and JMadeira did the field work. MM and PR did the magnetic studies. SM prepared the samples for geochemistry and geochronology. All authors wrote the manuscript.

SUPPORTING INFORMATION

Supplementary data are available at *GJIRAS* online.

Please note: Oxford University Press is not responsible for the content or functionality of any supporting materials supplied by the authors. Any queries (other than missing material) should be directed to the corresponding author for the paper.

CONFLICT OF INTEREST

The authors declare that they have no competing interests.

DATA AVAILABILITY

All data are incorporated into the paper and its online Supplementary Material. Additional data related to this study are available from the corresponding author, upon request.

REFERENCES

Arbaret, L., Diot, H. & Bouchez, J.L., 1996. Shape fabrics of particles in low concentration suspensions: 2D analogue experiments and application to tiling in magma, *J. Struct. Geol.,* **18**(7), 941–950..

Azéma, J., Fourcade, E. & de Wever, P., 1990. Découverte de Valanginien inférieur a Calpionelles à Maio (République du Cap Vert): discussion de l'âge des sédiments associés aux laves de type MORB de ce secteur de l'Atlantique Central, *C.R. Acad. Sci. Paris,* **310,** 277–283.

Baksi, A., 2003. Critical evaluation of $^{40}Ar/^{39}Ar$ ages for the Central Atlantic Magmatic Province: timing, duration and possible migration of magmatic centers, in The Central Atlantic Magmatic Province: insight from Fragments of Pangea, *AGU Monograph,* **136,** 77–90.

Baksi, A.K., 2006. *Guidelines for assessing the reliability of $^{40}Ar/^{39}Ar$ plateau ages: application to ages relevant to hotspot tracks*. html (accessed September 2024). http://www.mantleplumes.org/ArAr.html

Callot, J.P. & Guichet, X., 2003. Rock texture and magnetic lineation in dykes: a simple analytical model, *Tectonophysics,* **366**(3–4), 207–222..

Carmichael, I., Turner, F. & Verhoogen, J., 1974. *Igneous Petrology,* pp. 739, McGraw-Hill, New York.

Carvalho, J., Bonadio, R., Silveira, G., Lebedev, S., Mata, J., Arroucau, P., Meier, T. & Celli, N.L., 2019. Evidence for high temperature in the upper mantle beneath Cape Verde archipelago from Rayleigh-wave phase-velocity measurements, *Tectonophysics,* **770,** 228 225.

Casson, M., Bulot, L.G., Jeremiah, J. & Redfern, J., 2020. Deep sea rock record exhumed on oceanic volcanic islands: the Cretaceous sediments of Maio, Cape Verde, *Gondwana Res.,* **81,** 252–264.

Chadima, M. & Jelínek, V. 2008. Anisoft 4.2.–Anisotropy data browser, *Contrib. Geophys. Geod.,* **38**(Special Issue), 38–41.

Courtney, R.C. & White, R.S., 1986. Anomalous heat-flow and geoid across the Cape-Verde Rise—evidence for dynamic support from a thermal plume in the mantle, *Geophys. J. R. Astron. Soc.,* **87,** 815–867.

Dash, B.P., Ball, M.M., King, G.A., Butler, L.W. & Rona, P.A., 1976. Geophysical investigation of the Cape Verde archipelago, *J. Geophys. Res.,* **81,** 5249–5259.

Dragoni, M., Lanza, R. & Tallarico, A., 1997. Magnetic anisotropy produced by magma flow: theoretical model and experimental data from Ferrar dolerite sills (Antarctica), *Geophys. J. Int.,* **128**(1), 230–240.

Dunlop, D.J. & Özdemir, Ö., 1997. *Rock Magnetism Fundamentals and Frontiers,* Cambridge University Press, Cambridge.

Ellwood, B.B., 1978. Flow and emplacement direction determined for selected basaltic bodies using magnetic susceptibility anisotropy measurements, *Earth Planet. Sci. Lett.,* **41,** 254–264.

Fourcade, E., Azéma, J., de Wever, P. & Robert, B., 1990. Contribution à la datation de la croûte océanique de l'Atlantique central: age valanginien inférieur des basaltes océaniques et âge néocomien des calcaires Maiolica de Maio (Iles du Cap Vert), *Mar. Geol.,* **95**(1), 31–44.

Geoffroy, L., Aubourg, C., Callot, J.P. & Barrat, J.A., 2007. Mechanisms of crustal growth in large igneous provinces: the north Atlantic province as a case study, *Geol. Soc. Am. Special Paper,* **430,** 747–774.

Geoffroy, L., Callot, J.P., Aubourg, C. & Moreira, M., 2002**.** Magnetic plagioclase linear fabric discrepancy in dikes: a new way to define the flow vector using magnetic foliation, *Terra Nova,* **14**(3), 183–190**.**

González, P.J., Bagnardi, M., Hooper, A.J., Larsen, Y., Marinkovic, P., Samsonov, S.V. & Wright, T.J., 2015. The 2014–2015 eruption of Fogo volcano: geodetic modeling of Sentinel-1 TOPS interferometry, *Geophys. Res. Lett.,* **42,** 9239–9246. http://doi.org/10.1002/2015GL066003

Hayes, D. & Rabinowitz, P., 1975. Mesozoic magnetic lineations and the magnetic quiet zone off northwest Africa*, Earth Planet. Sci. Lett.,* **28,** 105–115. http://doi.org/10.1016/0012-821X(75)90217-4

Holm, P.M., Grandvuinet, T., Friis, J., Wilson, J.R., Barker, A.K. & Plesner, S., 2008. An ^{40}Ar-^{39}Ar study of the Cape Verde hot spot: temporal evolution in a semistationary plate environment, *J. geophys. Res.,* **113,** B08201. http://doi.org/10.1029/2007JB005339

Ildefonse, B., Launeau, P., Bouchez, J.-L. & Fernandez, A., 1992. Effect of mechanical interactions on the development of shape preferred orientations: a two-dimensional experimental approach, *J. Struct. Geol.,* **14**(1), 73–83. http://doi.org/10.1016/0191-8141(92)90146-N

Ivanov, A., He, H., Yang, L., Nikolaeva, I. & Palesskii, S., 2009. ^{40}Ar/^{39}Ar dating of intrusive magmatism in the Angara–Taseevskaya syncline and its implication for duration of magmatism of the Siberian traps, *J. Asian Earth Sci.,* **35,** 1–12.

Jelinek, V., 1978. Statistical Processing of Anisotropy of Magnetic Susceptibility Measured on Groups of Specimens, *Stud. Geophys. Geod*. **22,** 50–62.

Jelinek, V., 1981. Characterization of the magnetic fabric of rocks, *Tectonophysics,* **79,** T63–T67.

Kapicka, A., 1983. Irreversible changes of anisotropy of the magnetic susceptibility of rocks due to uniaxial pressure, *J. Geophys.,* **51,** 349–354.

Khan, M.A., 1962. Anisotropy of magnetic susceptibility of some igneous and metamorphic rocks, *J. geophys. Res.,* **67,** 2873–2885.

Klügel, A., Longpré, M.A., García-Cañada, L. & Stix, J., 2015. Deep intrusions, lateral magma transport and related uplift at ocean island volcanoes, *Earth planet. Sci. Lett.,* **431,** 140–149..

Knight, M.D. & Walker, G., 1988. Magma flow directions in dikes of the Koolau Complex, Oahu, determined from magnetic fabric studies, *J. Geophys. Res.,* **93**(B5), 4301–4319.

Koppers, A., 2002. ArArCALC-software for ^{40}Ar/^{39}Ar age calculations, *Comput. Geosci.,* **28,** 605–619..

Kruiver, P., Dekkers, M. & Heslop, D., 2001. Quantification of magnetic coercivity components by the analysis of acquisition curves of isothermal remanent magnetisation, *Earth planet. Sci. Lett.,* **189,** 269–276.

Launeau, P. & Robin, P.Y., 1996. Fabric analysis using the intercept method, *Tectonophysics,* **267,** 91–119.

Le Bas, M.J., Le Maitre, R.W., Streckeisen, A. & Zanettin, B., 1986. A chemical classification of igneous rocks based on the total alkali-silica diagram, *J. Petrol.,* **27,** 745–750.

Liu, X. & Zhao, D., 2014. Seismic evidence for a mantle plume beneath the Cape Verde hotspot, *Int. Geol. Rev.,* **56**(10), 1213–1225.

Liu, X. & Zhao, D., 2021. Seismic evidence for a plume-modified oceanic lithosphere–asthenosphere system beneath Cape Verde, *Geophys. J. Int.,* **225**(2), 872–886.

Madeira, J., Ramalho, R.S., Hoffmann, D.L., Mata, J. & Moreira, M., 2020. A geological record of multiple Pleistocene tsunami inundations in an oceanic island: the case of Maio, Cape Verde, *Sedimentology,* **67,** 1529–1552..

Mata, J. *et al.*, 2017. The 2014-15 eruption and the short-term geochemical evolution of the Fogo volcano (Cape Verde): evidence for small-scale mantle heterogeneity, *Lithos,* **288-289,** 91–107.

Mata, J., Moreira, M., Doucelance, R., Ader, M. & Silva, L.C., 2010. Noble gas and carbon isotopic signatures of Cape Verde oceanic carbonatites: implications for carbon provenance, *Earth planet. Sci. Lett.,* **291**(1–4), 70–83.

Mata, J. & Munhá, J., 2004. Madeira Island alkaline lava spinels: petrogenetic implications, *Mineral. Petrol.,* **81,** 85–111.

Min, K.W., Mundil, R., Renne, P.R. & Ludwig, K.R., 2000. A test for systematic errors in ^{40}Ar/^{39}Ar geochronology through comparison with U/Pb analysis of a 1.1-Ga rhyolite, *Geochim. Cosmochim. Acta,* **64,** 73–98.

Mitchell, J.G., Le Bas, M.J., Zielonka, J. & Furnes, H., 1983. On dating the magmatism of Maio, Cape Verde Islands, *Earth planet. Sci. Lett.,* **64,** 61–76.

Montelli, R., Nolet, G., Dahlen, F.A. & Masters, G., 2006. A catalogue of deep mantle plumes: new results from finite-frequency tomography, *Geochem. Geophys. Geosyst.,* **7,** Q11007.

Moreira, M., Geoffroy, L. & Pozzi, J.P., 1999. Ecoulement magmatique dans les dykes du point chaud des Açores: etude préliminaire par anisotropie de susceptibilité magnétique (ASM) dans l'île de San Jorge, *C. R. Acad. Sci. Ser. IIa: Sci. Terre Planets,* **329**(1), 15–22

Moreira, M., Geoffroy, L. & Pozzi, J.P., 2015. Magma flow pattern in dykes of the Azores revealed by anisotropy of magnetic susceptibility, *J. Geophys. Res. Solid Earth,* **120,** 662–690..

Mourão, C., Mata, J., Doucelance, R., Madeira, J., Millet, M.A. & Moreira, M., 2012. Geochemical temporal evolution of Brava Island magmatism: constraints on the variability of Cape Verde mantle sources and on carbonatite–silicate magma link, *Chem. Geol.,* **334,** 44–61.

Norman, M.D., Duncan, R.A. & Huard, J.J., 2010. Imbrium provenance for the Apollo 16 Descartes terrain: argon ages and geochemistry of lunar breccias 67016 and 67455, *Geochim. Cosmochim. Acta,* **74,** 763–783.

Paepe, P.D., Klerkx, J., Hertogen, J. & Plinke, P., 1974. Oceanic tholeiites on the Cape Verde Islands: petrochemical and geochemical evidence, *Earth planet. Sci. Lett.,* **22,** 347–354.

Philpotts, A.R. & Philpotts, D.E., 2007. Upward and downward flow in a camptonite dike as recorded by deformed vesicles and the anisotropy of magnetic susceptibility (AMS), *J. Volc. Geotherm. Res.,* **161**(1–2), 81–94.

Pim, J., Peirce, C., Watts, A.B., Grevemeyer, I. & Krabbenhoeft, A., 2008. Crustal structure and origin of the Cape Verde Rise, *Earth planet. Sci. Lett.,* **272**(1–2), 422–428.

Ramalho, R. *et al.*, 2017. Emergence and evolution of Santa Maria island (Azores)—the conundrum of uplifted islands revisited, *Geol. Soc. Am. Bull.,* **129,** 372–391.

Ramalho, R., Helffrich, G., Schmidt, D.N. & Vance, D., 2010. Tracers of uplift and subsidence in the Cape Verde archipelago, *J. Geol. Soc.,* **167**(3), 519–538.

Represas, P., Catalão, J., Montesinos, F.G., Madeira, J., Mata, J., Antunes, C. & Moreira, M., 2012. Constraints on the structure of Maio Island (Cape Verde) by a three-dimensional gravity model: imaging partially exhumed magma chambers, *Geophys. J. Int.,* **190,** 931–940.

Robertson, D.J. & France, D.E., 1994. Discrimination of remanence-carrying minerals in mixtures, using isothermal remanent magnetization acquisition curves, *Phys. Earth planet. Inter.,* **82**(3–4), 223–234.

Samrock, L.K., Hansteen, T.H., Dullo, W.C. & Wartho, J.A., 2022. Internal igneous growth, doming and rapid erosion of a mature ocean island: the Miocene evolution of Maio (Cabo Verde), *Int. J. Earth Sci. (Geol. Rundsch.),* **111,** 1129–1148.

Schaen, A. *et al.*, 2020. Interpreting and reporting ^{40}Ar/^{39}Ar geochronologic data, *Geol. Soc. Am. Bull.,* **133**(3–4), 461–487.

Serralheiro, A., 1970. Geologia da ilha de Maio (Cabo Verde). Lisboa, *103 pp. Junta de Investigação do Ultramar,* https://books.google.pt/books?id=NqonjwEACAAJ.

Silva, P.F., Marques, F.O., Machek, M., Henry, B., Hirt, A.M., Roxerová, Z., Madureira, P. & Vratislav, S., 2014. Evidence for non-coaxiality of ferrimagnetic and paramagnetic fabrics, developed during magma flow and cooling in a thick mafic dyke, *Tectonophysics,* **629,** 155–164.

Sleep, N.H., 1990. Hotspots and mantle plumes: some phenomenology, *J. geophys. Res.,* **95,** 6715–6736.

Stacey, F.D., 1960. Magnetic anisotropy of igneous rock, *J. geophys. Res.,* **65,** 2429–2442.

Steiger, R.H. & Jäger, E., 1977. Subcommission on geochronology: convention on the use of decay constants in geo- and cosmochronology, *Earth planet. Sci. Lett.,* **36,** 359–362.

Stillman, C., Furnes, H., LeBas, M., Robertson, A. & Zielonka, J., 1982. The geological history of Maio, Cape Verde Islands, *J. Geol. Soc.,* **139,** 347–361.

Symons, D., 1975. Age and flow direction from magnetic measurements on the historic Aiyansh flow, British Columbia, *J. geophys. Res.,* **80**(17), 2622–2626..

Tarling, D. & Hrouda, F., 1993. *The Magnetic Anisotropy of Rocks,* 81pp., Chapman and Hall, London.

Torres, P., Silva, L.C., Munhá, J., Caldeira, R., Mata, J. & Tassinari, C., 2010. Petrology and Geochemistry of lavas from Sal Island: implications for the variability of the Cape Verde magmatism, *Comunicações Geológicas,* **97,** 35–62. https://hdl.handle.net/10400.9/1142

Villaseca, C. *et al.*, 2025. The old central igneous complexes of Sal, Boa Vista and Maio islands: implications for 17 Ma of isotopic evolution of the Cape Verde archipelago, *Lithos,* **498–499,** 107 975.

Vinnik, L., Silveira, G., Kiselev, K., Farra, V., Weber, W. & Stutzmann, E., 2012. Cape Verde hotspot from the upper crust to the top of the lower mantle, *Earth planet. Sci. Lett.,* **319–320,** 259–268..

Warwick, W., Michael, K. & Aubourg, C., 2014. Magma flow in dyke swarms of the Karoo LIP: implications for the mantle plume hypothesis, *Gondwana Res.,* **25**(2), 736–755.